

Asymptotically-Flat Black Hole Solutions in Symmergent Gravity ^a

Beyhan Pulice,^{1,†} Reggie C. Pantig,^{2,‡} Ali Övgün,^{3,§} and Durmuş Demir^{1,¶}

¹Faculty of Engineering and Natural Sciences, Sabancı University, 34956 İstanbul, Turkey

²Physics Department, Mapúa University, 658 Muralla St., Intramuros, Manila 1002, Philippines

³Physics Department, Eastern Mediterranean University,
Famagusta, 99628 North Cyprus, via Mersin 10, Turkey

(Dated: March 6, 2024)

Symmergent gravity is an emergent gravity model with an $R + R^2$ curvature sector and an extended particle sector having new particles beyond the known ones. With constant scalar curvature, asymptotically flat black hole solutions are known to have no sensitivity to the quadratic curvature term (coefficient of R^2). With variable scalar curvature, however, asymptotically-flat symmergent black hole solutions turn out to explicitly depend on the quadratic curvature term. In the present work, we construct asymptotically-flat symmergent black holes with variable scalar curvature and use its evaporation, shadow, and deflection angle to constrain the symmergent gravity parameters. Concerning their evaporation, we find that the new particles predicted by symmergent gravity, even if they do not interact with the known particles, can enhance the black hole evaporation rate. Concerning their shadow, we show that statistically significant symmergent effects are reached at the 2σ level for the observational data of the Event Horizon Telescope (EHT) on the Sagittarius A* supermassive black hole. Concerning their weak deflection angle, we reveal discernible features for the boson-fermion number differences, particularly at large impact parameters. These findings hold the potential to serve as theoretical predictions for future observations and investigations on black hole properties.

PACS numbers: 95.30.Sf, 04.70.-s, 97.60.Lf, 04.50.Kd

Keywords: Symmergent gravity; Black holes; Hawking radiation; Black hole shadow; Black hole deflection angle

I. INTRODUCTION

In the Wilsonian sense, quantum field theories (QFTs) are characterized by a classical action and an ultraviolet (UV) cutoff Λ . Quantum loops lead to effective QFTs with loop momenta cut at Λ . Effective QFTs generally suffer from UV over-sensitivity problems: the scalar and gauge boson masses receive $\mathcal{O}(\Lambda^2)$ corrections. The vacuum energy, on the other hand, gets corrected by $\mathcal{O}(\Lambda^4)$ and $\mathcal{O}(\Lambda^2)$ terms. The gauge symmetries get explicitly broken. The question is simple: Can gravity emerge in a way that restores the explicitly broken gauge symmetries? Asking differently, can gravity emerge in a way alleviates the UV over-sensitivities of the effective QFT? This question has been answered affirmatively [1, 2], with the constructions of a gauge symmetry-restoring emergent gravity model (see also [3, 4]). This model, briefly called as *symmergent gravity*, has been built by the observation that, in parallel with the introduction of Higgs field to restore gauge symmetry for a massive vector boson (with Casimir invariant mass) [5–7], spacetime affine curvature can be introduced to restore gauge symmetries for gauge bosons with loop-induced (Casimir non-invariant) masses proportional to the UV cutoff Λ [1, 2]. Symmergent gravity is emergent general relativity (GR) with a quadratic curvature term ($R + R^2$ gravity) and new particles beyond the known ones. Its curvature (as well as particle) sector exhibits distinctive signatures, as revealed in recent works on inflation [8] and static black hole spacetimes [9–12].

Scientists predicted the existence of shadow of black holes a long time ago [13–15], but it wasn't until recently that the Event Horizon Telescope (EHT) team was able to acquire the first direct photograph of a black hole [16]. This photograph specifically depicted the shadow of M87*, a supermassive black hole at the center of the Messier 87 galaxy and then and Sagittarius A* [16, 17]. This remarkable discovery implies that we may soon be able to obtain valuable information on black holes, such as their mass, spin, and charge, in a systematic manner [18, 19]. We can gather data to derive these characteristics by studying black hole shadows, which are essentially dark representations of their event horizon, and photon rings, which are dazzling images formed by photons circling around black holes [20–22], which are especially noteworthy since they provide accurate gravity constraints in the strong-field regime [21, 23–53]. These discrepancies could be caused by many reasons linked with several alternative theories of gravity [54–68] or the surrounding astrophysical conditions in which the black hole is located [69–76]. Therefore, it becomes crucial to investigate modified gravity theories and establish constraints by utilizing the black hole's shadow alongside astrophysical data, such as observations from telescopes like EHT.

^a Dedicated to Durmuş Demir (1967–2024), our supervisor, candid friend, and guiding light. His unwavering supports always led our way.

[†] beyhan.pulice@sabanciuniv.edu

[‡] rcpantig@mapua.edu.ph

[§] ali.ovgun@emu.edu.tr

[¶] durmus.demir@sabanciuniv.edu

In the present work, we construct and analyze asymptotically-flat, static, spherically-symmetric symmergent gravity black holes. In the case of constant scalar curvature, the quadratic curvature term (coefficient of R^2) is known not to affect the asymptotically flat spacetimes [77–79]. In the case of variable scalar curvature, however, there arise asymptotically-flat solutions with explicit dependence on the quadratic curvature term [80] (see also [81, 82]). In Sec. II, we give a detailed discussion of the symmergent gravity [1, 2] in regarding its new particles sector (Sec. IIA) and its curvature sector (Sec. IIB). In Sec. III, we construct asymptotically-flat, static, spherically symmergent gravity black holes with variable scalar curvature. Our analysis goes beyond [80] as we consider both positive and negative values of the boson-fermion number difference (or the parameter γ in [80]). In both cases, we demonstrate asymptotic flatness of the metric, with approximate analytic calculations and the exact numerical solutions. In Sec. IV, we compute the Hawking temperature using the tunneling method and state that black hole evaporation could be accelerated if there exist considerable new light particles. In Sec. V, we analyze how the symmergent black hole can be probed via its shadow cast and weak deflection angle. And we have shown that the symmergent effects on the shadow are small, and the weak deflection angle can distinguish different boson-fermion number differences at fairly large impact factors. In Sec. VI, we conclude.

II. SYMMERGENT GRAVITY

In this section, we give a brief description of symmergent gravity in terms of its fundamental parameters. The starting point is quantum field theories (QFTs). Quantum fields are endowed with mass and spin as their Casimir invariants of the Poincaré group. Fundamentally, QFTs are intrinsic to the flat spacetime simply because they rest on a Poincaré-invariant (translation-invariant) vacuum state [83, 84]. Flat spacetime means the total absence of gravity, and its incorporation necessitates the QFTs to be carried into curved spacetime. But this carriage is hampered by Poincaré breaking in curved spacetime [84, 85], and this hamper and the absence of a quantum theory of gravity [86] together lead one to emergent gravity framework [87–89] as a viable approach.

In general, the loss of Poincaré invariance could be interpreted as the emergence of gravity form within the QFT [90]. In a QFT, curvature can emerge at the Poincaré breaking sources. One natural Poincaré breaking source is the hard momentum cutoff on the QFT. Indeed, an ultraviolet (UV) cutoff Λ [91] limits momenta p_μ within $-\Lambda^2 \leq \eta^{\mu\nu} p_\mu p_\nu \leq \Lambda^2$ interval as the intrinsic validity edge of the QFT [91]. Under the loop corrections under the cutoff Λ , the action $S[\eta, \phi, V]$ of a QFT of scalars S and gauge bosons V_μ receives the correction (with $(+, -, -, -)$ metric signature appropriate for QFTs)

$$\delta S[\eta, \phi, V] = \int d^4x \sqrt{-\eta} \left\{ -c_O \Lambda^4 - \sum_i c_{m_i} m_i^2 \Lambda^2 - c_S \Lambda^2 S^\dagger S + c_V \Lambda^2 V_\mu V^\mu \right\}, \quad (1)$$

in which $\eta_{\mu\nu}$ is the flat metric, m_i stands for the mass of a QFT field ψ_i (summing over all the fermions and bosons), and c_O , c_m , c_S and c_V are respectively the loop factors describing the quartic vacuum energy correction, quadratic vacuum energy correction, quadratic scalar mass correction, and the loop-induced gauge boson mass [92, 93]. As revealed by the gauge boson mass term $c_V \Lambda^2 V_\mu V^\mu$, the UV cutoff Λ breaks gauge symmetries explicitly since Λ is not a particle mass, that is, Λ is not a Casimir invariant of the Poincaré group. The loop factor c_V (and c_S) depends on the details of the QFT. (It has been calculated for the standard model gauge group in [2, 3].)

In Sakharov's induced gravity [87, 88], the UV cutoff Λ is associated with the Planck scale, albeit with explicitly broken gauge symmetries and Planckian-size cosmological constant and scalar masses. In recent years, Sakharov's setup has been approached from a new perspective in which priority is given to the prevention of the explicit gauge symmetry breaking [1, 2]. For this aim, one first takes the effective QFT in (1) to curved spacetime of a metric $g_{\mu\nu}$ such that the gauge boson mass term is mapped as $c_V \Lambda^2 \eta^{\mu\nu} V_\mu V_\nu \rightarrow c_V V_\mu (\Lambda^2 g^{\mu\nu} - R^{\mu\nu}(g)) V_\nu$ in agreement with the fact that the Ricci curvature $R^{\mu\nu}(g)$ of the metric $g_{\mu\nu}$ can arise only in the gauge sector via the covariant derivatives [1–3]. One next inspires from the Higgs mechanism to promote the UV cutoff Λ to an appropriate spurion field. Indeed, in parallel with the introduction of the Higgs field to restore gauge symmetry for a massive vector boson (Poincare-conserving mass) [5–7], one can introduce spacetime affine curvature to restore gauge symmetries for gauge bosons with loop-induced (Poincare-breaking) masses proportional to Λ [1, 2, 94, 95]. Then, one is led to the map

$$\Lambda^2 g^{\mu\nu} \rightarrow \mathbb{R}^{\mu\nu}(\Gamma), \quad (2)$$

in which $\mathbb{R}^{\mu\nu}(\Gamma)$ is the Ricci curvature of the affine connection $\Gamma_{\mu\nu}^\lambda$, which is completely independent of the curved metric $g_{\mu\nu}$ and its Levi-Civita connection [94–96]. This map is analog of the map $M_V^2 \rightarrow \phi^\dagger \phi$ of the vector boson mass M_V (Poincare conserving) into the Higgs field ϕ . Under the map (2), the effective QFT in (1) takes the form

$$\delta S[g, \phi, V, \mathbb{R}] = \int d^4x \sqrt{-\eta} \left\{ -\frac{c_O}{16} \mathbb{R}^2 - \sum_i \frac{c_{m_i}}{4} m_i^2 \mathbb{R} - \frac{c_S}{4} \mathbb{R} S^\dagger S + c_V V_\mu (\mathbb{R}^{\mu\nu}(\Gamma) - R^{\mu\nu}(g)) V_\nu \right\}, \quad (3)$$

in which $\mathbb{R} \equiv g^{\mu\nu}\mathbb{R}_{\mu\nu}(\Gamma)$ is the affine scalar curvature [2], which tends to the usual metrical scalar curvature under the affine dynamics to be discussed in Sec. II B below. This metric-Palatini theory contains both the metrical curvature $R(g)$ and the affine curvature $\mathbb{R}(\Gamma)$. From the second term, Newton's gravitational constant G_N is read out to be

$$G_N^{-1} = 4\pi \sum_i c_{m_i} m_i^2 \xrightarrow{\text{one loop}} \frac{1}{8\pi} \text{str}[\mathcal{M}^2], \quad (4)$$

where \mathcal{M}^2 is the mass-squared matrix of all the fields in the QFT spectrum. In the one-loop expression, $\text{str}[\dots]$ stands for super-trace namely $\text{str}[\mathcal{M}^2] = \sum_i (-1)^{2s_i} (2s_i + 1) \text{tr}[\mathcal{M}^2]_{s_i}$ in which $\text{tr}[\dots]$ is the usual trace (including the color degrees of freedom), s_i is the spin of the QFT field ψ_i ($s_i = 0, 1/2, \dots$), and $[\mathcal{M}^2]_{s_i}$ is the mass-squared matrix of the fields having that spin (like mass-squared matrices of scalars ($s_i = 0$), fermions ($s_i = 1/2$) and so on). One keeps in mind that $\text{tr}[\dots]$ encodes degrees of freedom g_i (like color and other degrees of freedom) of the particles.

A. First Prediction of Symmergence: Naturally-Coupled New Particles

It is clear that the known particles (the quarks, leptons, gauge bosons, and the Higgs boson in the Standard Model (SM)) can generate Newton's constant in (4) neither in size ($\text{str}[\mathcal{M}^2] \sim (\text{TeV})^2$ in the SM) nor in sign ($\text{str}[\mathcal{M}^2] < 0$ in the SM). It is thus necessary to introduce new particles. What is interesting about these new particles is that they do not have to couple to the known SM particles since the only constraint on them is the super-trace in (4) [1, 2]. They may not interact with the SM particles, but they may interact, too. If they interact, there is no symmetry principle or selection rule that forces their coupling strengths to be of the SM size (as in supersymmetry, extra dimensions, and technicolor). To see this, it suffices to consider renormalizable interactions of the form

$$\mathcal{L}_{int} = \lambda_{HH'} (H^\dagger H) \cdot (H'^\dagger H'), \quad (5)$$

in which H is the SM Higgs field, and H' stands for new scalar fields. The main point is that the coupling constant $\lambda_{HH'}$ is forced to take a value $\lambda_{HH'} \sim \lambda_{SM}$ in supersymmetry, extra dimensions, and technicolor due to their symmetry structures correlating the SM fields and the new fields. (In supersymmetry, for instance, superpartners are the new fields that interact with the SM fields with SM-sized couplings due to supersymmetry transformations.) Here, λ_{SM} is a typical SM coupling such as the top Yukawa coupling $\lambda_t \approx 1$, and under such sizable couplings, the H' -loop corrections to the Higgs mass

$$\delta m_H^2 \propto \lambda_{HH'} m_{H'}^2 \log \frac{m_{H'}^2}{m_H^2}, \quad (6)$$

become too large to remain within the experimental error bars when $m_{H'} \gg m_H$. As a matter of fact, supersymmetry and other new physics models have been sidelined based on these corrections in that the LHC experiments seem to be near the $m_{H'} \gg m_H$ regime run after run.

Symmergence is entirely different. The reason is that there is no symmetry structure correlating the SM fields and the new fields, so the coupling constant $\lambda_{HH'}$ in (5) can take any perturbative value: $\lambda_{HH'} = 0 \dots \lambda_{SM}$. These new fields we call *symmerons* to distinguish them from new physics models with sizable couplings to the SM [1, 2]. Broadly speaking, symmerons can come in three classes [1–4, 97]:

1. *Visible Symmerons* are those new particles that are endowed with the SM charges and are allowed, therefore to interact with the SM with sizable couplings (like $\lambda_{HH'} \sim \lambda_{SM}$). These particles weigh necessarily at the SM scale if they are not to destabilize the SM Higgs sector via the Higgs mass corrections they induce (like δm_H^2). The LHC results and results from various dark matter searches seem to disfavor such symmerons.
2. *Dark Symmerons* are those new particles that are neutral under the SM charges and are allowed therefore to interact with the SM with weak (or feeble) couplings in the range $\lambda_{HH'} \lesssim \lambda_{max}$ within which the H' -loop corrections in (6) remain small enough to keep the SM Higgs sector stable. In fact, as suggested by (6), one can take $\lambda_{max} \simeq \frac{m_H^2}{m_{H'}^2}$ as an optimal coupling strength for such symmerons.
3. *Black Symmerons* are those new particles that do not couple to the SM at all (like $\lambda_{HH'} = 0$). These symmerons form a secluded sector that interacts with the SM via only gravity. This kind of symmerons (and the feebly-coupled dark symmerons) broadly agree with most observations.

The built-in immunity of symmergence to coupling strengths between the SM and the requisite new fields is an important property. This picture is in overall agreement with the existing astrophysical [98, 99], cosmological [100] and collider [101] searches (see also [97]). The symmerons are a prediction of symmergence, and we shall discuss their impact on black hole physics in the next section.

B. Second Prediction of Symmergence: $R + R^2$ Gravity with Loop-Induced Parameters

The action (3) remains stationary against variations in the affine connection provided that

$$\Gamma \nabla_\lambda \mathbb{D}_{\mu\nu} = 0, \quad (7)$$

such that $\Gamma \nabla_\lambda$ is the covariant derivative of the affine connection $\Gamma_{\mu\nu}^\lambda$, and

$$\mathbb{D}_{\mu\nu} = \left(\frac{1}{16\pi G} + \frac{c_S}{4} S^\dagger S + \frac{c_O}{8} g^{\alpha\beta} \mathbb{R}_{\alpha\beta}(\Gamma) \right) g_{\mu\nu} - c_V V_\mu V_\nu, \quad (8)$$

is the field-dependent metric. The motion equation (7) implies that $\mathbb{D}_{\mu\nu}$ is covariantly-constant with respect to $\Gamma_{\mu\nu}^\lambda$. In solving (7), it is legitimate to make the expansions

$$\Gamma_{\mu\nu}^\lambda = {}^g \Gamma_{\mu\nu}^\lambda + \mathcal{O}(G_N), \quad (9)$$

and

$$\mathbb{R}_{\mu\nu}(\Gamma) = R_{\mu\nu}(g) + \mathcal{O}(G_N), \quad (10)$$

since the Planck scale in (4) is the largest scale. In these expansions, though not made explicit, both $\Gamma_{\mu\nu}^\lambda$ and $\mathbb{R}_{\mu\nu}(\Gamma)$ contain pure derivative terms at the next-to-leading $\mathcal{O}(G_N)$ order [3, 4]. The expansion in (9) ensures that the affine connection $\Gamma_{\mu\nu}^\lambda$ is solved algebraically order by order in G_N despite the fact that its motion equation (7) involves its own curvature $\mathbb{R}_{\mu\nu}(\Gamma)$ through $\mathbb{D}_{\mu\nu}$ [94, 95]. The expansion (10), on the other hand, ensures that the affine curvature $\mathbb{R}_{\mu\nu}(\Gamma)$ is equal to the metrical curvature $R_{\mu\nu}(g)$ up to a doubly-Planck suppressed remainder. In essence, what happened is that the affine dynamics took the affine curvature \mathbb{R} from its UV value Λ_ϕ^2 in (2) to its IR value R in (10). This way, the GR emerges holographically [102, 103] via the affine dynamics such that loop-induced gauge boson masses get erased, and scalar masses get stabilized by the curvature terms. This mechanism renders effective field theories natural regarding their destabilizing UV sensitivities [1, 2]. It gives rise to a new framework in which (i) the gravity sector is composed of the Einstein-Hilbert term plus a curvature-squared term, and (ii) the matter sector is described by an \overline{MS} -renormalized QFT [1–3]. We call this framework gauge symmetry-restoring emergent gravity or simply *symmergent gravity* to distinguish it from other emergent or induced gravity theories in the literature.

It is worth noting that symmergent gravity is not a loop-induced curvature sector in curved spacetime [88, 104]. In contrast, symmergent gravity arises when the flat spacetime effective QFT is taken to curved spacetime [1–3] in a way restoring the gauge symmetries broken explicitly by the UV cutoff. All of its couplings are loop-induced parameters deriving from the particle spectrum of the QFT (numbers and masses of particles). It is with these loop features that the GR emerges. In fact, the metric-Palatini action (3) reduces to the metrical gravity theory

$$\begin{aligned} \int d^4x \sqrt{-g} \left\{ -\frac{\mathbb{R}(g)}{16\pi G_N} - \frac{c_O}{16} (\mathbb{R}(g))^2 + \frac{c_S}{4} S^\dagger S \mathbb{R}(g) + c_V \text{tr} [V^\mu (\mathbb{R}_{\mu\nu}(\Gamma) - R_{\mu\nu}({}^g \Gamma)) V^\nu] \right\} \\ \xrightarrow{\text{equation (10)}} \int d^4x \sqrt{-g} \left\{ -\frac{R}{16\pi G_N} - \frac{c_O}{16} R^2 - \frac{c_S}{4} S^\dagger S R + \mathcal{O}(G_N) \right\}, \end{aligned} \quad (11)$$

after replacing the affine curvature $\mathbb{R}_{\mu\nu}(\Gamma)$ with its solution in (10). Of the parameters of this emergent GR action, Newton's constant G_N was already defined in (4). The loop factor c_S depends on the underlying QFT. (It reads $c_S \simeq 0.29$ in the standard model.) The loop factor c_O , which was associated with the quartic (Λ^4) corrections in the flat spacetime effective QFT in (1), turned to the coefficient of quadratic-curvature (R^2) term in the symmergent GR action in (11). At one loop, it takes the value

$$c_O = \frac{n_B - n_F}{128\pi^2}, \quad (12)$$

in which n_B (n_F) stands for the total number of bosonic (fermionic) degrees of freedom in the underlying QFT (including the color degrees of freedom). Both the n_B bosons and n_F fermions contain not only the known standard model particles but also the completely new particles. As was commented just above (7), it is a virtue of symmergence that these new particles do not have to couple to the known ones non-gravitationally.

In the above, we have consistently dropped the total vacuum energy, assuming that the cosmological constant problem has been solved by an appropriate method. Saying differently, we have assumed that the tree-level vacuum energy and

logarithmic loop corrections left over (power-law Λ^4 corrections have been converted to curvature) from symmergence have been alleviated by an appropriate mechanism.

Symmergence makes gravity emerge from within the flat spacetime effective QFT. Fundamentally, as follows from the action (1), Newton's constant G_N in (4) and the quadratic curvature coefficient c_O in (12) transpired in the flat spacetime effective QFT from the matter loops. (The loop factor c_S and similar parameters involve matter fields.) A glance at the second line of (11) reveals that symmergent gravity is an $R + R^2$ gravity theory with the non-zero cosmological constant. In fact, it can be put in the form

$$S = -\frac{c_O}{16} \int d^4x \sqrt{-g} (R^2 + 6\gamma G_N^{-1} R), \quad (13)$$

after leaving aside the scalars S and the other matter fields, after switching to $(-, +, +, +)$ metric signature (appropriate for the black hole analysis in the sequel), and after introducing the constant

$$\gamma = -\frac{1}{6\pi c_O} = -\frac{64\pi}{3(n_B - n_F)}, \quad (14)$$

where c_O was defined in equation (12) above. Here, one recalls that $(n_B - n_F)_{SM} = -62$ and hence $(\gamma)_{SM} \approx 1$. However, as already discussed in Sec. II A, the SM spectrum is insufficient for inducing the gravitational constant in (4), and thus, it is necessary to introduce new fields beyond the SM. The new fields cause (i) Newton's constant to be induced as in (4), (ii) $|n_B - n_F|$ to be larger or smaller than $|(n_B - n_F)_{SM}|$ depending on the mass spectrum ($n_B - n_F = 0$ corresponds to Bose-Fermi balance as in supersymmetric QFTs and nullifies the quadratic curvature term), and (iii) $\text{sign}(n_B - n_F)$ to be positive ($n_B > n_F$) or negative ($n_B < n_F$) depending again on the mass spectrum. All this means that γ can deviate from its SM value significantly in both the positive and negative directions.

III. ASYMPTOTICALLY-FLAT BLACK HOLE SPACETIME IN SYMMERGENT GRAVITY

The symmergent gravitational action in (13) remains stationary against variations in the metric provided that the Einstein field equations

$$(R + 3\gamma G_N^{-1})R_{\mu\nu} - \frac{1}{4}(R + 6\gamma G_N^{-1})Rg_{\mu\nu} - (\nabla_\mu \nabla_\nu - \square g_{\mu\nu})R = 0, \quad (15)$$

hold as motion equation for the metric $g_{\mu\nu}$. These equations possess static, spherically-symmetric, asymptotically-flat solutions. Such solutions with constant scalar curvature ($R = \text{constant}$) turn out to be insensitive to the quadratic-curvature term in (13). In other words, such solutions bear no sensitivity to the loop factor c_O , and they cannot thus probe vacuum symmergent gravity. (This insensitivity is a common feature of all $R + R^2$ gravity theories [77–79], and gets lost in the presence of the cosmological constant [9–12].)

The Einstein field equations (15) possess also static, spherically-symmetric, asymptotically-flat solutions with variable scalar curvature ($R = \text{variable}$) [80] (see also [81, 82]). These solutions show direct sensitivity to the quadratic-curvature term in (13). They are thus sensitive to c_O , and have the ability to probe symmergent gravity. In fact, introducing the dimensionless black hole mass $M \rightarrow G_N^{1/2} M \equiv M$ and dimensionless radial distance $r \rightarrow G_N^{-1/2} r \equiv r$, $r \rightarrow G_N^{-1/2} r \equiv r$, recently it has been shown that the metric [81]

$$ds^2 = -(1 - \varphi(r))\Psi(r)dt^2 + \frac{dr^2}{(1 + \varphi(r))\Psi(r)} + r^2 d\Omega^2, \quad (16)$$

satisfies the Einstein field equations (15) at the linear order in $\varphi(r)$ provided that the differential equation [81] (see also [80, 82])

$$(r^2 \Psi(r) \varphi'(r))' = \gamma r^2 \varphi(r), \quad (17)$$

is satisfied for both $\gamma > 0$ (as was assumed in [81]) and $\gamma < 0$ (as will be considered additionally in the present work). Here, the Schwarzschild lapse function

$$\Psi(r) = 1 - \frac{2M}{r}, \quad (18)$$

has a zero (horizon) at $r = 2M$, as expected. Singularity structure of the spacetime (16) is revealed by the Kretschmann scalar

$$R_{\mu\nu\sigma\rho} R^{\mu\nu\sigma\rho} = \frac{48M^2}{r^6} (1 + 2\varphi(r)), \quad (19)$$

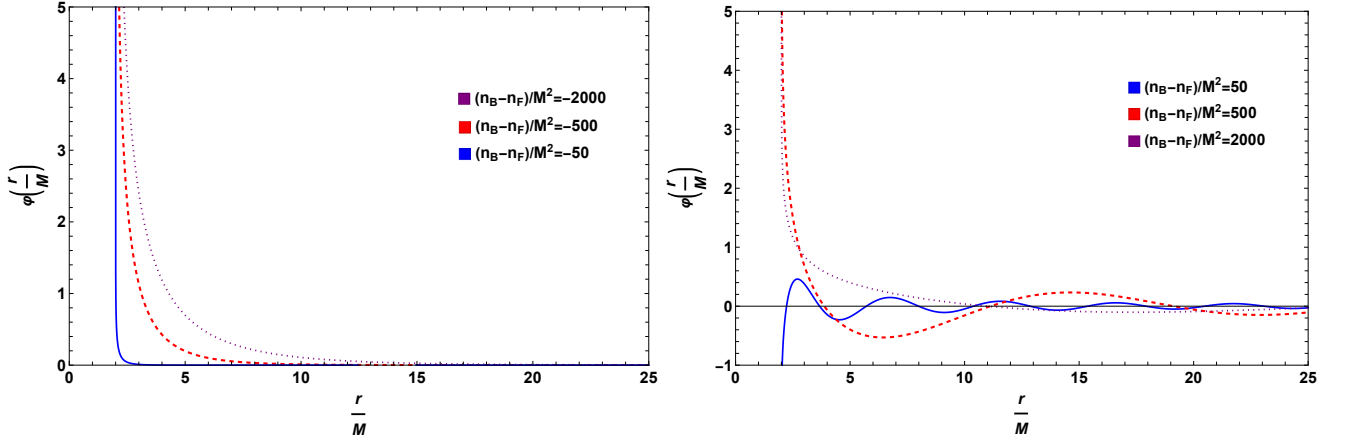


FIG. 1. Exact numerical solution of φ from the defining equation (17) as a function of the radial distance r/M for selected negative values of $n_B - n_F$ ($\gamma > 0$) (left panel) and positive values of $n_B - n_F$ ($\gamma < 0$) (right panel). In view of the validity domain of the metric (16), it is clear that essentially only $\varphi(r)$ at radial distances $r \gtrsim 2$ are allowed (above the Schwarzschild horizon).

which is seen to differ from the usual Schwarzschild value by $\varphi(r)$.

Our analyses below of various physical quantities rest on the exact solution of the φ -equation in (17) in which the Schwarzschild lapse function $\Psi(r)$ is treated exactly. In fact, the $\varphi(r)$ in Fig. 1 is obtained by such an exact numerical solution. For clarity and definiteness, however, it proves useful to illustrate these exact numerical solutions with approximate large- r asymptotes. In this regard, large- r behavior of $\varphi(r)$ is given by

$$\varphi(r) = \begin{cases} \frac{e^{-\sqrt{\gamma}r}}{\sqrt{\gamma}r} & \gamma > 0 \\ \frac{\cos(\sqrt{|\gamma|r})}{\sqrt{|\gamma|r}} & \gamma < 0 \end{cases} \quad (20)$$

in the limit $r \gg 2M$ so that $\Psi(r) \approx 1$ in equation (17) above. The first line ($\gamma > 0$) of this equation was already derived in [80]. The second line, our derivation, is also important since the parameter γ , as defined in (14), is positive for $n_B < n_F$ and negative for $n_B > n_F$. As revealed by (20), the metric in (16) is asymptotically-flat for both $\gamma > 0$ and $\gamma \leq 0$ but its approach to the flatness is different in the two cases. In view of these asymptotic solutions, the metric (16) can be put in a more definitive form as

$$ds^2 = -A(r)dt^2 + \frac{dr^2}{B(r)} + C(r)(d\theta^2 + \sin^2\theta d\phi^2), \quad (21)$$

with the metric potentials

$$A(r) = \left(1 - \frac{2M}{r}\right) \left(1 - \frac{e^{-r\sqrt{\gamma}}}{r\sqrt{\gamma}}\right), \quad (22)$$

$$B(r) = \left(1 - \frac{2M}{r}\right) \left(1 + \frac{e^{-r\sqrt{\gamma}}}{r\sqrt{\gamma}}\right), \quad (23)$$

$$C(r) = r^2 \left(1 - \frac{e^{-r\sqrt{\gamma}}}{r\sqrt{\gamma}}\right). \quad (24)$$

for $\gamma > 0$, and

$$A(r) = \left(1 - \frac{2M}{r}\right) \left(1 - \frac{\cos(\sqrt{|\gamma|r})}{r\sqrt{|\gamma|}}\right), \quad (25)$$

$$B(r) = \left(1 - \frac{2M}{r}\right) \left(1 + \frac{\cos(\sqrt{|\gamma|r})}{r\sqrt{|\gamma|}}\right), \quad (26)$$

$$C(r) = r^2 \left(1 - \frac{\cos(\sqrt{|\gamma|r})}{r\sqrt{|\gamma|}}\right) \quad (27)$$

for $\gamma < 0$. The plots in Fig. 2 and Fig. 3 represent these metric potentials for $r \gtrsim 2$ (above the Schwarzschild horizon).

In Fig. 2, we depict the exact solutions of $A(r)$ (left panel) and $B(r)$ (right panel) for $n_B - n_F = -50, -500$ and -2000 . This figure confirms the large- r exponential behaviors of $A(r)$ in (22) and $B(r)$ in (23). It is clear that different $n_B - n_F$ curves rapidly merge and asymptote to unity – the flat spacetime. In parallel with Fig. 2, we depict in Fig. 3 the exact solutions of $A(r)$ (left panel) and $B(r)$ (right panel) for $n_B - n_F = 50, 200$ and 2000 . Needless to say, this figure conforms with the large- r sinusoidal behaviors of $A(r)$ in (25) and $B(r)$ in (26). It is clear that different $n_B - n_F$ values merge gradually (not rapidly) and asymptote to unity – the flat spacetime.

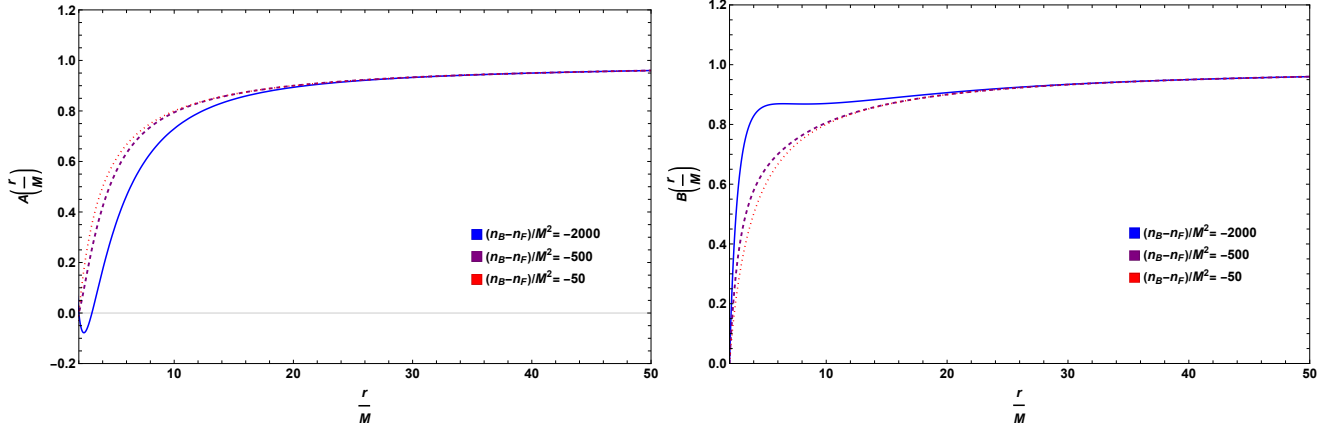


FIG. 2. Exact solutions of the metric potentials (22) and (23) as functions of the radial distance r for selected negative values of $(n_B - n_F)/M^2$ ($\gamma > 0$). These solutions are reliable mainly at distances $r \gtrsim 2$ in view of the validity of the metric (16).

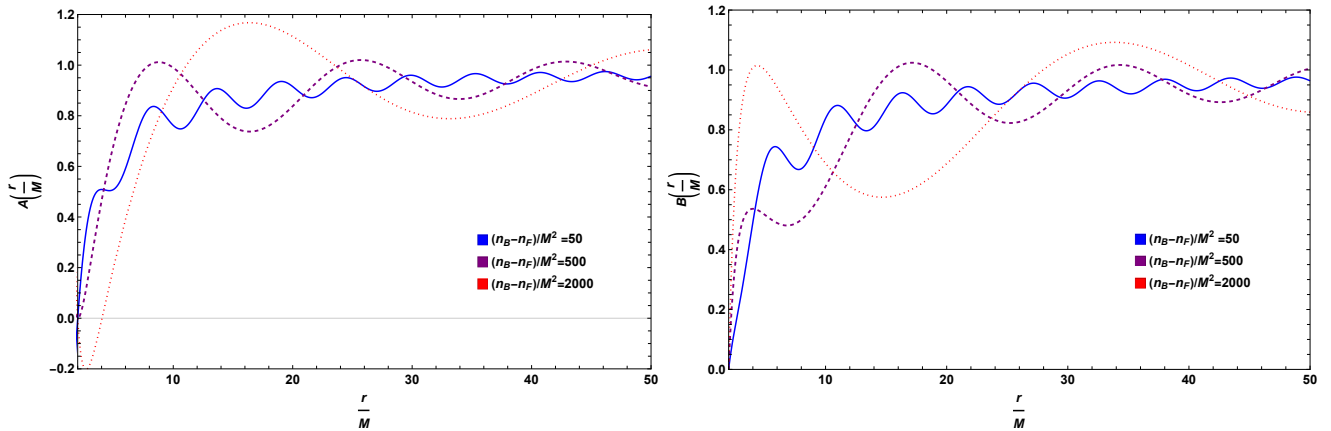


FIG. 3. Exact solutions of the metric potentials (25) and (26) as functions of the radial distance r for selected positive values of $(n_B - n_F)/M^2$ ($\gamma \leq 0$). These solutions are reliable mainly at distances $r \gtrsim 2$ in view of the validity of the metric (16).

The exact numerical solutions above and their congruence with the asymptotic solutions show that the symmergent spacetime with the metric (17) asymptotes to flat spacetime in both $n_B - n_F < 0$ ($\gamma > 0$) and $n_B - n_F > 0$ ($\gamma < 0$) cases.

In Fig. 4, we give the allowed regions in r vs $n_B - n_F$ plane (shaded in blue). These regions are determined by imposing $r \gtrsim 2$ (see Fig. 1 above) from the validity of the metric (16) and by imposing also $0 < A(r) < 1$ from the causality. The left-panel and right-panel correspond to $\gamma > 0$ and $\gamma < 0$, respectively. In the analyses below, r and $n_B - n_F$ values falling in the gray regions will not be considered. It is clear that the allowed region extends over a semi-infinite values in both r and $n_B - n_F$ directions.

IV. TUNNELING OF SYMMERONS AND OTHER PARTICLES: HAWKING TEMPERATURE

One of the key predictions of symmergence is that there necessarily exist new particles beyond the known SM spectrum, and these new particles do not have to interact non-gravitationally with the SM particles [97]. These new particles, the

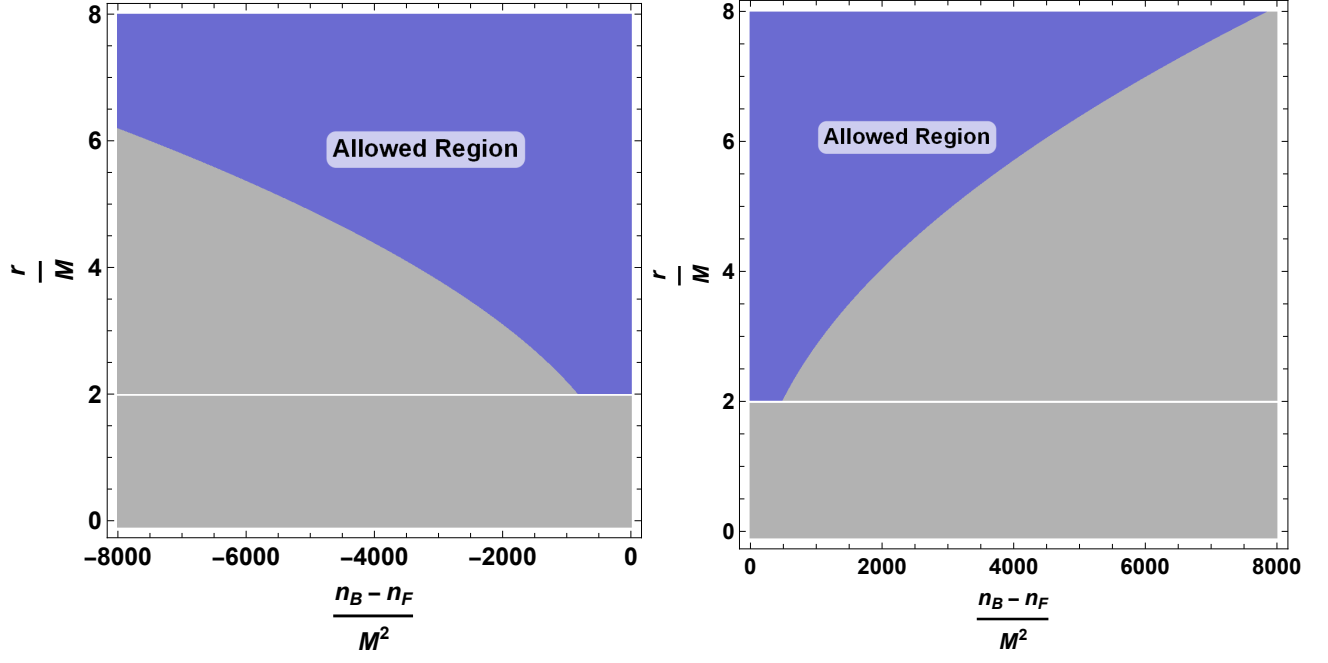


FIG. 4. Allowed ranges of r and $n_B - n_F$ after imposing $r \gtrsim 2$ from the validity of the metric (16) and after imposing also $0 < A(r) < 1$ from causality. The left-panel (right-panel) corresponds to negative (positive) $n_B - n_F$ values. The white straight line at $r = 2$ indicates the Schwarzschild horizon.

symmerons of Sec. II A, form a naturally-coupled sector [97], and this sector could be visible (having SM-sized couplings to the SM), dark (having feeble interactions with the SM) or even black (having zero interactions with the SM). But, irrespective of their nature, symmerons couple to gravity and, to this end, black holes provide a viable environment to investigate their effects (on top of the $n_B - n_F$ dependence of γ in (14)).

One way to observe symmerons is to measure the Hawking radiation from the symmergent black hole. More precisely, the evaporation rate of the symmergent black hole can reveal if there are light symmerons in the spectrum. Indeed, Hawking radiation is formed by the particles tunneling through the effective potential barrier at the horizon, and these particles can be the SM particles like the photon or featherweight symmerons. In fact, symmerons can form a dark Hawking radiation as they do not have to couple to the SM spectrum.

Tunneling of particles from black holes and the resulting Hawking radiation have been studied for scalars [105–114], fermions [115–122] and vectors [123–129]. Tunneling offers more than just a valuable method to verify the thermodynamic properties of black holes in that it also serves as an alternative conceptual approach to grasp the fundamental physical process behind black hole radiation. In general, tunneling methods involve the computation of the imaginary part of the action associated with the classically forbidden process of s-wave emission across the black hole horizon. This imaginary part is directly linked to the Boltzmann factor, which characterizes the probability of emission at the Hawking temperature. Here, we shall compute Hawking radiation as the tunneling of vector particles (like the photon and light vector symmerons) in static, spherically-symmetric, asymptotically-flat symmergent black holes with metric (21). The motion equation for an Abelian massive vector V_μ of mass M_V is given by

$$\frac{1}{\sqrt{-g}} \partial_\mu (\sqrt{-g} V^{\nu\mu}) - \frac{M_V^2 c^2}{\hbar^2} V^\nu = 0, \quad (28)$$

in which $V_{\nu\mu} = \partial_\nu V_\mu - \partial_\mu V_\nu$ is the field-strength tensor of the massive vector V_μ . We will solve this equation by the WKB method [130] and, to this end, we will suppress the speed of light c but keep \hbar to perform the WKB expansion. In fact, by labeling the components of V_μ as $V_\mu = (V_0, V_1, V_2, V_3)$, the Proca equation (28) can be decomposed as

$$\begin{aligned} \sqrt{\frac{B}{A}} \frac{1}{C \sin \theta} \left[\partial_r \left(-\sqrt{\frac{B}{A}} C \sin \theta (\partial_t V_1 - \partial_r V_0) \right) + \partial_\theta \left(-\frac{\sin \theta}{\sqrt{AB}} (\partial_t V_2 - \partial_\theta V_0) \right) \right. \\ \left. + \partial_\phi \left(-\frac{1}{\sqrt{AB} \sin \theta} (\partial_t V_3 - \partial_\phi V_0) \right) \right] - \frac{M_V^2}{\hbar^2} \left(-\frac{V_0}{A} \right) = 0, \quad (29) \end{aligned}$$

$$\begin{aligned} \sqrt{\frac{B}{A}} \frac{1}{C \sin \theta} \left[\partial_t \left(\sqrt{\frac{B}{A}} C \sin \theta (\partial_t V_1 - \partial_r V_0) \right) + \partial_\theta \left(\sqrt{AB} \sin \theta (\partial_r V_2 - \partial_\theta V_1) \right) \right. \\ \left. + \partial_\phi \left(\frac{\sqrt{AB}}{\sin \theta} (\partial_r V_3 - \partial_\phi V_1) \right) \right] - \frac{M_V^2}{\hbar^2} (B V_1) = 0, \end{aligned} \quad (30)$$

$$\begin{aligned} \sqrt{\frac{B}{A}} \frac{1}{C \sin \theta} \left[\partial_t \left(\frac{\sin \theta}{\sqrt{AB}} (\partial_t V_2 - \partial_\theta V_0) \right) + \partial_r \left(-\sqrt{AB} \sin \theta (\partial_r V_2 - \partial_\theta V_1) \right) \right. \\ \left. + \partial_\phi \left(\sqrt{\frac{A}{B}} \frac{1}{C \sin \theta} (\partial_\theta V_3 - \partial_\phi V_2) \right) \right] - \frac{m^2}{\hbar^2} \left(\frac{V_2}{C} \right) = 0, \end{aligned} \quad (31)$$

and

$$\begin{aligned} \sqrt{\frac{B}{A}} \frac{1}{C \sin \theta} \left[\partial_t \left(\sqrt{\frac{1}{AB}} \frac{1}{\sin \theta} (\partial_t V_3 - \partial_\phi V_0) \right) + \partial_r \left(-\frac{\sqrt{AB}}{\sin \theta} (\partial_r V_3 - \partial_\phi V_1) \right) \right. \\ \left. + \partial_\theta \left(-\sqrt{\frac{A}{B}} \frac{1}{C \sin \theta} (\partial_\theta V_3 - \partial_\phi V_2) \right) \right] - \frac{M_V^2}{\hbar^2} \left(\frac{V_3}{C \sin^2 \theta} \right) = 0. \end{aligned} \quad (32)$$

In the usual sense, the WKB wavefunction [130]

$$(V_0, V_1, V_2, V_3) = (v_0, v_1, v_2, v_3) \exp \left(\frac{i}{\hbar} I(t, r, \theta, \phi) \right), \quad (33)$$

can be determined order by order in \hbar by expanding the action as

$$I(t, r, \theta, \phi) = I_0(t, r, \theta, \phi) + \hbar I_1(t, r, \theta, \phi) + O(\hbar^2), \quad (34)$$

in which I_0 is the classical action, I_1 is the one-loop correction, and so on. In the classical limit ($\hbar \rightarrow 0$), the classical action I_0 becomes the dominant piece (the semi-classical wavefunction) and admits the decomposition [105–109]

$$I = -\hbar \omega t + \hbar \int^r \kappa(r) dr, \quad (35)$$

as because it satisfies the Hamilton-Jacobi equation with energy $\hbar \omega = -\frac{\partial I_0}{\partial t}$ and momentum $\hbar \kappa(r) = \frac{\partial I_0}{\partial r}$.

Under the decomposition (35), the Proca equations (29),(30),(31) and (32) take the compact form

$$(v_0, v_1, v_2, v_3)^T \cdot \mathbb{C} = 0, \quad (36)$$

in which the coefficient matrix

$$\mathbb{C} = \begin{pmatrix} \frac{(B\kappa^2 + M_V^2)}{A} & \frac{\omega B \kappa}{A} & 0 & 0 \\ \frac{\omega B \kappa}{A} & \frac{B(\omega^2 - M_V^2 A)}{A} & 0 & 0 \\ 0 & 0 & \frac{\omega^2 - A(M_V^2 + B\kappa^2)}{AC} & 0 \\ 0 & 0 & 0 & \frac{\csc^2 \theta (\omega^2 - A(M_V^2 + B\kappa^2))}{AC} \end{pmatrix} \quad (37)$$

is set by the classical action in (35). The vector field components (v_0, v_1, v_2, v_3) can take non-zero values if the coefficient matrix is not invertible, namely if it has zero determinant

$$\text{Det}[\mathbb{C}] = 0 \implies \omega^2 - A(M_V^2 + B\kappa^2) = 0, \quad (38)$$

so that $\kappa^2 = (\omega^2 - M_V^2 A)/AB$. This solution for momentum $\hbar \kappa$ leads to the classical action

$$I_0(t, r) = \hbar \omega t \pm \hbar \int^r d\tilde{r} \sqrt{\frac{\omega^2 - M_V^2 A(\tilde{r})}{A(\tilde{r})B(\tilde{r})}}, \quad (39)$$

whose value around the horizon $r = r_H$ should give the Euclidean action describing the barrier region. By definition, $A(r = r_H) = 0$ and $B(r = r_H) = 0$ at the horizon, and they can therefore be expanded thereabouts as

$$\begin{aligned} A(r) &= A'(r_H)(r - r_H) + \mathcal{O}\left[(r - r_H)^2\right], \\ B(r) &= B'(r_H)(r - r_H) + \mathcal{O}\left[(r - r_H)^2\right], \end{aligned} \quad (40)$$

so that the classical action (39) takes the form

$$I_0(t, r) = \hbar\omega t \pm \hbar \int dr \frac{\omega}{\sqrt{A'(r_H)B'(r_H)}(r - r_H)}, \quad (41)$$

and its integration by the residue theorem gives

$$I_0(t, r) = \hbar\omega t \pm \frac{i\pi\hbar\omega}{\sqrt{A'(r_H)B'(r_H)}}, \quad (42)$$

with a + (−) sign corresponding to outgoing (incoming) massive vector waves. With this solution for the classical action, the WKB wavefunction in (33) takes the form

$$V_\mu = v_\mu \exp\left(i\omega t \mp \frac{\pi\omega}{\sqrt{A'(r_H)B'(r_H)}}\right), \quad (43)$$

up to one-loop corrections, which we neglect. From this wavefunction follows the emission probability [115]

$$P_{em,\mu} = |v_\mu|^2 \exp\left\{-\frac{2\pi\omega}{\sqrt{A'(r_H)B'(r_H)}}\right\}, \quad (44)$$

and the absorption probability

$$P_{ab,\mu} = |v_\mu|^2 \exp\left\{\frac{2\pi\omega}{\sqrt{A'(r_H)B'(r_H)}}\right\}, \quad (45)$$

One notes that the imaginary part of the action is the same for both incoming and outgoing solutions. Now, we want to define the decay rate of the black hole. To do that, we need to normalize the emission probability with respect to a given probability distribution. This is accomplished in reference [131] by adding a constant part to the classical action and choosing that constant part in a way normalizing the absorption probability to unity [111, 132]. In our derivation, the same result is obtained by normalizing the emission probability to the absorption probability, namely

$$\Gamma_\mu = \frac{P_{em,\mu}}{P_{ab,\mu}} = \exp\left\{-\frac{4\pi\omega}{\sqrt{A'(r_H)B'(r_H)}}\right\}, \quad (46)$$

and from this rate formula, one reads the Hawking temperature, which is inversely linked with the Boltzmann factor β , $T_H = \beta^{-1}$ as

$$T_H = \frac{\sqrt{A'(r_H)B'(r_H)}}{4\pi}, \quad (47)$$

which differs from the Hawking temperature of Schwarzschild black hole by the presence of the conformal factor $\varphi(r)$ in the metric (16). In fact, it takes the explicit form

$$(T_H)_{\gamma>0} = \frac{M}{2\pi r_H^2} \sqrt{1 - \frac{e^{-2\sqrt{\gamma}r_H} (r_H + \sqrt{\gamma}r_H^2 - 2M(2 + \sqrt{\gamma}r_H))^2}{4M^2\gamma r_H^2}}, \quad (48)$$

for $n_B < n_F$ ($\gamma > 0$), and

$$(T_H)_{\gamma\leq 0} = \frac{M}{2\pi r_H^2} \sqrt{1 - \frac{\left((r_H - 4M) \cos(\sqrt{|\gamma|r_H}) + \sqrt{\gamma}r_H(r_H - 2M) \sin(\sqrt{|\gamma|r_H})\right)^2}{4M^2\gamma r_H^2}}, \quad (49)$$

for $n_B > n_F$ ($\gamma \leq 0$). We plot the Hawking temperature in Fig. 5 as a function of radial distance r for $n_B - n_F < 0$ (left panel) and $n_B - n_F > 0$ (right panel). As is seen from the left panel, when $n_B - n_F < 0$, the Hawking temperature makes a peak and then falls off exponentially at large r such that the larger the $|n_B - n_F|$ smaller the peak temperature and farther the peak position. These peaks can indicate negative $n_B - n_F$ if detected by black hole observations.

The Hawking temperature for $n_B - n_F > 0$, as indicated by the right panel of Fig. 5, decreases with r exhibiting a periodic pattern. The fall is gradual. Thus, it becomes easier to distinguish different $n_B - n_F$ values compared to $n_B - n_F < 0$ case in the left panel. The periodic behavior can serve as the indicator of positive $n_B - n_F$ if it can be detected by black hole observations.

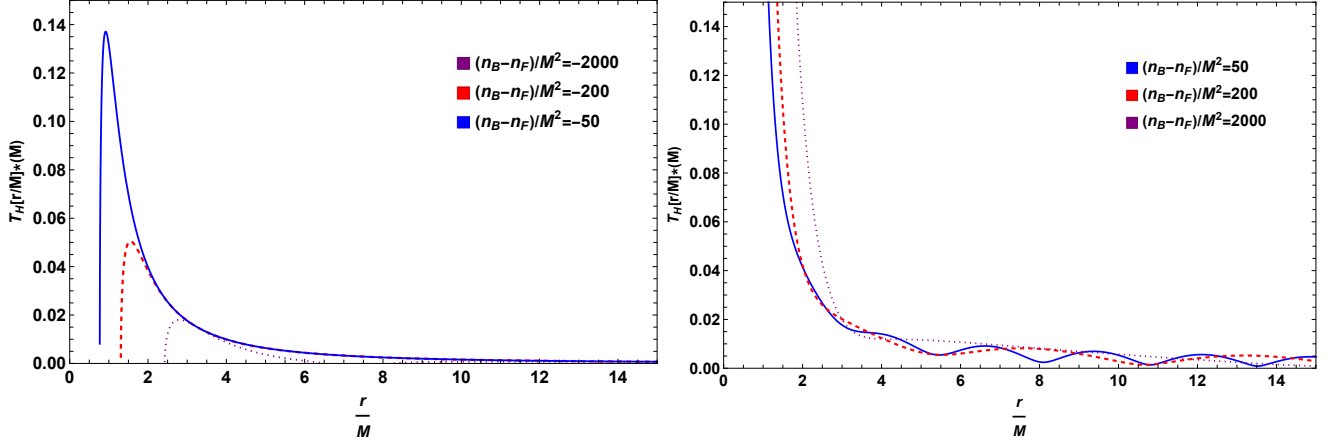


FIG. 5. Hawking temperature as a function of the radial distance r for selected negative values of $n_B - n_F$ ($\gamma > 0$)(left panel) and positive values of $n_B - n_F$ ($\gamma < 0$)(right panel).

The vector field Hawking temperature in Fig. 5 illustrates the contribution of one single flavor. But, in general, black holes emit not only the photons but also neutrinos [133]. In symmergent gravity, the emission spectrum can be multifarious as it can now involve symmerons [1–3]. Indeed, as discussed in detail in Sec. II A, symmerons can be dark (or even black), and it can be hard to detect them at collider experiments or dark matter sector searches. But, irrespective of their nature, they can contribute to the Hawking radiation and affect the evaporation rate of the black hole. To be definitive, the Hawking emission rate of any particle species i is given by [133–137]

$$\frac{d^2 N_i}{d\omega dt} = \frac{n_i \sigma_i \omega^2}{2\pi^2 (e^{\omega/T_H} \pm 1)}, \quad (50)$$

in which n_i is the number of degrees of freedom of the species i , $+$ ($-$) stands for fermions (bosons), σ_i is the absorption cross section, and T_H is the Hawking temperature of the black hole. This rate conforms with the black hole decay rate in (46) except for the quantum-statistics factors. The absorption cross section σ_i is given by $\sigma_i = \pi E^{-2} \Gamma_i$, where Γ_i is the greybody factor [138]. The greybody factor is a measure of deviations from the perfect black body spectrum in (46) and results from the backscattering of the particles under the strong gravity of the black hole. To a good approximation, the absorption cross-section σ_i can be identified with the geometrical cross-section of the black hole's photon sphere [139]

$$\sigma_i \approx \pi R_{sh}^2 \quad (51)$$

as a universal formula for all species. In parallel with the change of the particle number in (50), a black hole emits energy E at a rate [140]

$$\frac{d^2 E}{d\omega dt} = \frac{2\pi^2 \sigma_i \omega^3}{(e^{\omega/T_H} \pm 1)} \quad (52)$$

in which the absorption cross section σ_i can be identified with (51). This energy emission rate we plot in Fig. 6 for $n_B - n_F < 0$ (left panel) and $n_B - n_F > 0$ (right panel). It is clear that the energy emission rate makes a peak a specific frequency such that when $n_B - n_F$ decreases in a negative direction, the peak gets suppressed and shifts to smaller ω values. In contrast, when $n_B - n_F$ increases in a positive direction, the peak gets pronounced and shifts to larger ω values.

Depicted in Fig. 7 is the particle emission rate as a function of the frequency ω for $n_B - n_F < 0$ (left panel) and $n_B - n_F > 0$ (right panel). It exhibits a similar behavior as the energy emission rate in Fig. 6 in that the rate at which a given particle species is emitted makes a peak at a specific frequency. The peak decreases with the decreasing values

of negative $n_B - n_F$ and shifts to lower frequencies. In parallel, the peak increases with the increasing values of positive $n_B - n_F$ and shifts to higher frequencies. It is clear that the positions of the peaks could give information about whether or not the bosonic degrees of freedom in the Universe are larger than the fermionic ones. It is worth noting that positive $n_B - n_F$ should be significantly large for the peaks to show noticeable shifts (the right panels of both Fig. 6 and Fig. 7).

In view of the symmergent gravity explored, it proves useful to explicate the symmeron contributions, and, to this end, the total particle emission rate proves to be a useful quantity. Indeed, as follows from the individual rates in (50), the total emission rate consists of all species of any spin [133]

$$\frac{dN}{dt} = \sum_{i=\gamma,\nu,\text{symmerons}} \int \frac{n_i \sigma_i \omega^2 d\omega}{\pi^2 (e^{\omega/T_H} \pm 1)} \approx \sum_{i=\gamma,\nu,\text{symmerons}} \frac{k_i \zeta(3)}{\pi} n_i T_H^3 R_{sh}^2 = \frac{\zeta(3)}{\pi} T_H^3 R_{sh}^2 \left(13 + 2n_B^{(0)} + \frac{3}{2}n_F^{(0)} \right) \quad (53)$$

with the dominance of light (massless) particles as because contributions of massive particles get suppressed as e^{-mass/T_H} . In this expression, $\zeta(3) \approx 1.202$ (Riemann zeta-function) and $k_i = 2(3/2)$ for bosons (fermions). In the last equality, photon ($n_i = 2$) plus neutrino ($n_i = 6$) contributions sum up to 13. This SM rate is extended by the contributions of $n_B^{(0)}$ massless bosonic symmerons plus $n_F^{(0)}$ massless fermionic symmerons. It is all clear that symmerons increase the particle emission rate (black hole evaporation) in direct proportion to number of massless symmerons. This effect on the total emission rate might be determined or inferred by observing a given black hole at its different phases of evolution in a certain environment. One thus concludes that possible observation of the black hole evaporation can give information about new massless/light particles beyond the known particles in the SM. And symmergent gravity predicts the existence of such particles and also predicts that these particles may not interact at all with the known particles non-gravitationally [1–3].

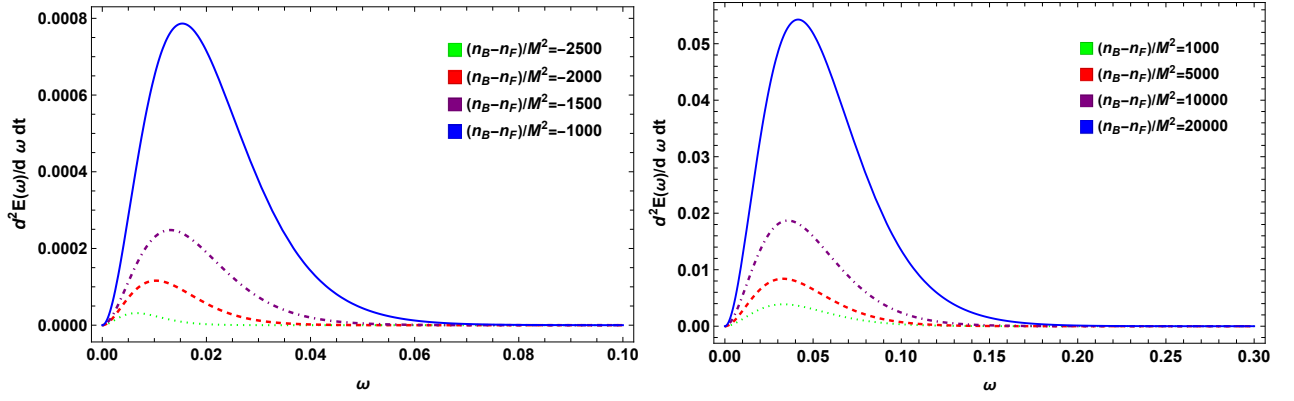


FIG. 6. The energy emission rate in (52) as a function of frequency for $n_B - n_F < 0$ (left panel) and $n_B - n_F > 0$ (right panel). The movement of the peak position is a distinctive feature.

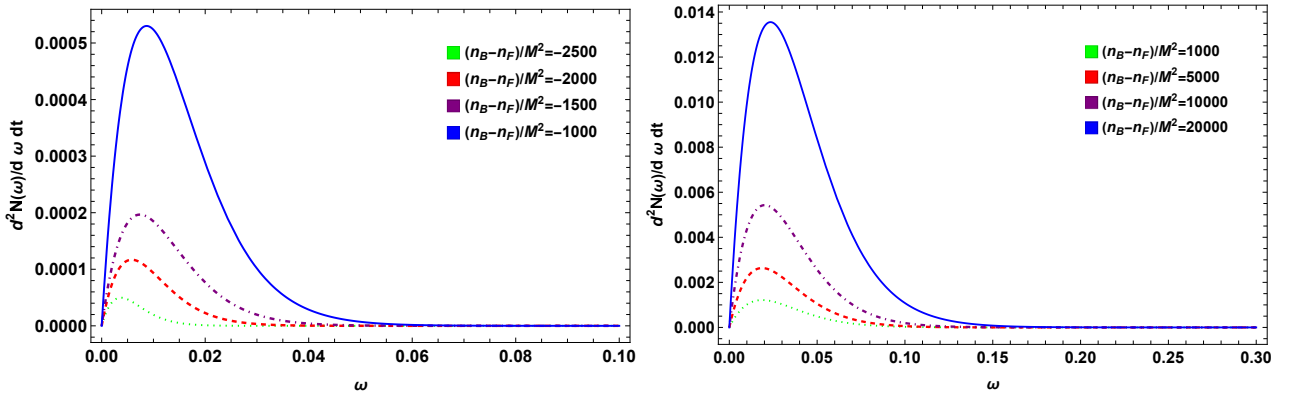


FIG. 7. The particle emission rate in (50) as a function of frequency for $n_B - n_F < 0$ (left panel) and $n_B - n_F > 0$ (right panel). The movement of the peak position is a distinctive feature.

V. PHOTON SPHERE, SHADOW CAST AND WEAK DEFLECTION ANGLE OF THE SYMMERGENT BLACK HOLE

In this section, we analyze the photon sphere and shadow cast of the symmergent black hole. Given the spherical symmetry of the metric in (16), it suffices to analyze null geodesics in the equatorial plane ($\theta = \pi/2$). The null geodesic Lagrangian

$$\mathcal{L} = \frac{1}{2}g_{\mu\nu}\dot{x}^\mu\dot{x}^\nu = \frac{1}{2}\left(-A(r)\dot{t}^2 + \frac{\dot{r}^2}{B(r)} + C(r)\dot{\phi}^2\right), \quad (54)$$

leads to the energy

$$E = A(r)\frac{dt}{d\lambda}, \quad (55)$$

and the angular momentum

$$L = C(r)\frac{d\phi}{d\lambda}, \quad (56)$$

as two constants of motion. Their ratio gives the impact parameter

$$b = \frac{L}{E} = \frac{C(r)}{A(r)}\frac{d\phi}{dt}, \quad (57)$$

involving the coordinate angular velocity $d\phi/dt$. Using the impact parameter b , the null geodesic $ds^2 = 0$ enables us to relate r to ϕ as [141]

$$\left(\frac{dr}{d\phi}\right)^2 = B(r)C(r)\left(\frac{h(r)^2}{b^2} - 1\right), \quad (58)$$

after defining

$$h(r)^2 = \frac{C(r)}{A(r)}, \quad (59)$$

for simplicity. The null geodesic $r = r(\phi)$ remains stable if these two conditions are satisfied: The first condition is $dr/d\phi = 0$, and it implies $h(r_{\text{PS}}) = b$ as follows from (58). The second condition is $d^2r/d\phi^2 = 0$, and it requires $\frac{d}{dr}\left(\frac{A(r)}{C(r)}\right)\Big|_{r=r_{\text{PS}}} = 0$ as follows again from (58). These two conditions lead to the relation

$$C(r_{\text{PS}})A'(r_{\text{PS}}) - C'(r_{\text{PS}})A(r_{\text{PS}}) = 0, \quad (60)$$

as the equation defining the radius of stable sphere $r = r_{\text{PS}}$. For both $\gamma > 0$ and $\gamma < 0$, one solution of equation (60) is $r_{\text{PS}} = 3M$, which corresponds to the Schwarzschild part of the metric (16). The other solution is a nontrivial function of γ , and it reads $r_{\text{PS}} = \text{LambertW}(1)\sqrt{\gamma}$ for $\gamma > 0$. For $\gamma < 0$, a closed analytic solution is not available and it becomes necessary to resort to numerical techniques. The two cases are depicted in Fig. 8 for both $n_B - n_F < 0$ (left panel) and $n_B - n_F > 0$ (right panel). As follows from the left panel, the second photon sphere occurs at larger and larger radii for smaller and smaller negative $n_B - n_F$. The right panel, on the other hand, reveals that the second photon sphere occurs at a radius $r_{\text{PS}} \approx 6.3M$ at large $n_B - n_F$. Consequently, photons form two stable spheres for both $n_B - n_F < 0$ and $n_B - n_F > 0$, and the radii of these spheres can be a distinctive signature of the symmergent gravity.

The non-rotating symmergent black hole under concern can produce only a circular shadow silhouette. The shadow is caused by photons falling within the photon sphere of radius $r = r_{\text{PS}}$. For the Schwarzschild black hole, the photon radius is $r_{\text{PS}} = 3M$, and its shadow has the radius $R_{\text{sh}} = 3\sqrt{3}M$. The shadow radius coincides with the critical impact parameter $b = b_{\text{crit}}$ at which photons are just at the threshold of getting caught by the gravity of the black hole. Needless to say, R_{sh} is nothing but the gravitationally lensed image of the photon sphere of radius $r = r_{\text{PS}}$ [142]. In symmergent gravity, the shadow radius is given by

$$R_{\text{sh}} = \sqrt{\frac{C(r_{\text{PS}})}{A(r_{\text{PS}})}} \quad (61)$$

and it can be determined analytically for $\gamma > 0$ and $\gamma < 0$ separately. However, the analytic expressions are too lengthy to be suggestive and therefore it proves convenient to proceed with the numerical calculations. It is clear that R_{sh} varies

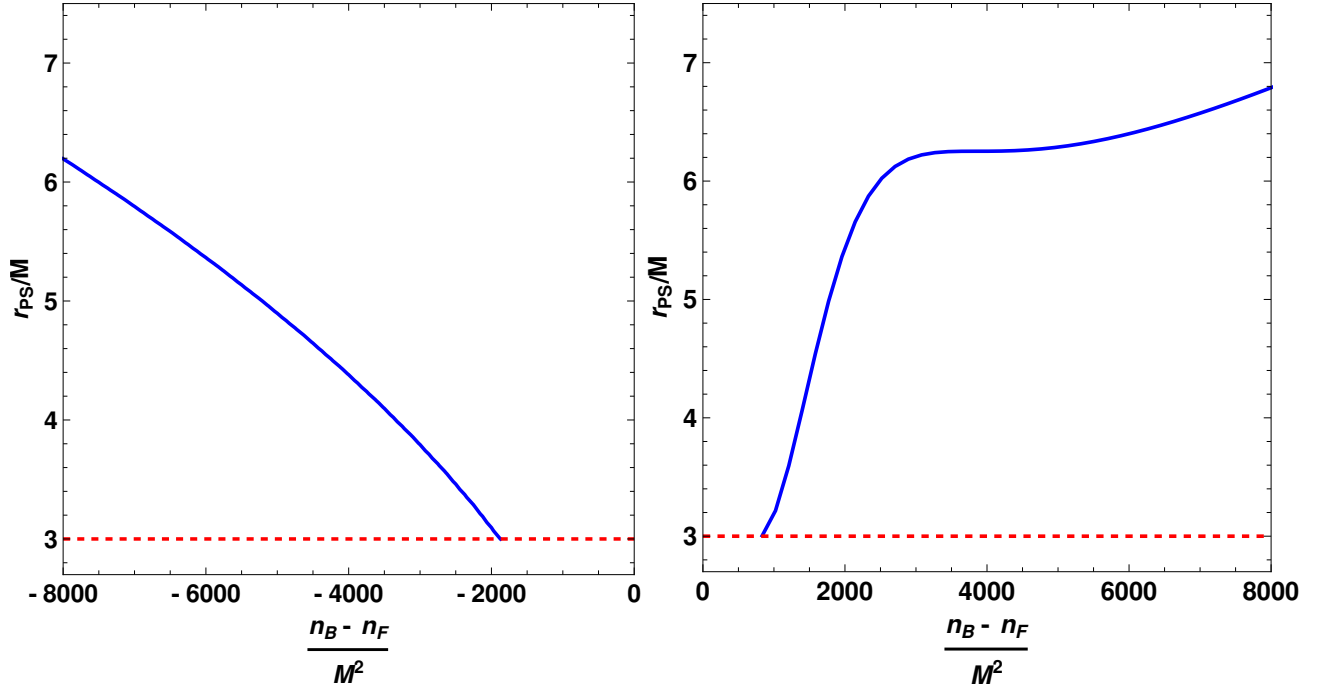


FIG. 8. The photon sphere behavior as a function of $n_B - n_F$ for $n_B - n_F < 0$ (left panel) and $n_B - n_F > 0$ (right panel). The red-dashed line at $r = 3M$ is the photon sphere radius for the Schwarzschild metric. The blue line, falling in the allowed domains in Fig. 4, are the photon sphere radius characterizing the non-Schwarzschild part of the metric (16).

Black hole	Mass (M_\odot)	Angular diameter: $2\alpha_{\text{sh}}$ (μas)	Distance (kpc)	Schw. dev. (2σ)
Sgr. A*	$4.3 \pm 0.013 \times 10^6$ (VLTI)	48.7 ± 7 (EHT)	8.277 ± 0.033	$3\sqrt{3}[1 + (-0.06 \pm 0.065)]$
M87*	$6.5 \pm 0.90 \times 10^9$	42 ± 3	16800	$3\sqrt{3}(1 \pm 0.17)$

TABLE I. Observational constraints on the mass, angular shadow radius, distance, and Schwarzschild deviation of the supermassive black holes Sgr. A* and M87*.

with $n_B - n_F$ through the photon sphere radius r_{PS} in Fig. 8. We plot in Fig. 9 the shadow radius of the symmergent black hole as a function of $n_B - n_F$ for $n_B - n_F < 0$ (left panel) and $n_B - n_F > 0$ (right panel). The two panels are nearly mirror-symmetric to each other. (Actually, the R_{sh} lies in different $n_B - n_F$ ranges.) Superimposed on the R_{sh} plot in Fig. 9 are the observational results on the Sgr. A* tabulated in Table I. (The bounds from M87* are much milder [21].) The observation of the exponential and inverse relationship displayed by $n_B - n_F$ continues to captivate our interest, regardless of the variation range of the parameters. In Fig. 9, we present the upper boundaries of $|n_B - n_F|$; these values have been contextualized based on the Event Horizon Telescope (EHT) observations. As per the statistical interpretation at a confidence level (C.L.) of 68% as delineated in the study by Vagnozzi et al. (2022) [21], the upper constraint for $n_B - n_F$ manifests as -1700 and -2100 for the left diagram and 1300 and 1000 for the right diagram. As the figure reveals, symmergent effects fall in the 2σ band, with a tiny tail in the 1σ band. The R_{sh} nears the Schwarzschild value of $R_{\text{sh}} = 3\sqrt{3}$ around $n_b - n_f \approx -2000$ (left) and $n_b - n_f \approx 1100$ (right). These minimal values fall into the allowed domains (blue) in Fig. 4. In view of these small 1σ tails, future higher-precision observations on the supermassive and other black holes could be expected to bound the symmergent parameters.

Lastly, we analyze the deflection angle numerically in weak field limits from the symmergent black hole described by the metric (16). For the symmergent metric (16), the bending angle in gravitational lensing is given by [143–145]

$$\delta(r_0) = \int_{r_0}^{\infty} \frac{2}{\sqrt{B(r)C(r)}} \frac{dr}{\sqrt{\frac{C(r)}{C(r_0)} \frac{A(r_0)}{A(r)} - 1}} - \pi, \quad (62)$$

where r_0 is the closest approach distance of the light ray to the symmergent black hole. In the weak deflection lensing, $r_0 \gg 2M$ so that $\delta \ll 1$. We perform this integration numerically and plot the results in Fig. 10 for both $n_B - n_F < 0$ (left panel) and $n_B - n_F > 0$ (right panel). As the figure suggests, the deflection angle is similar in the two cases, with a

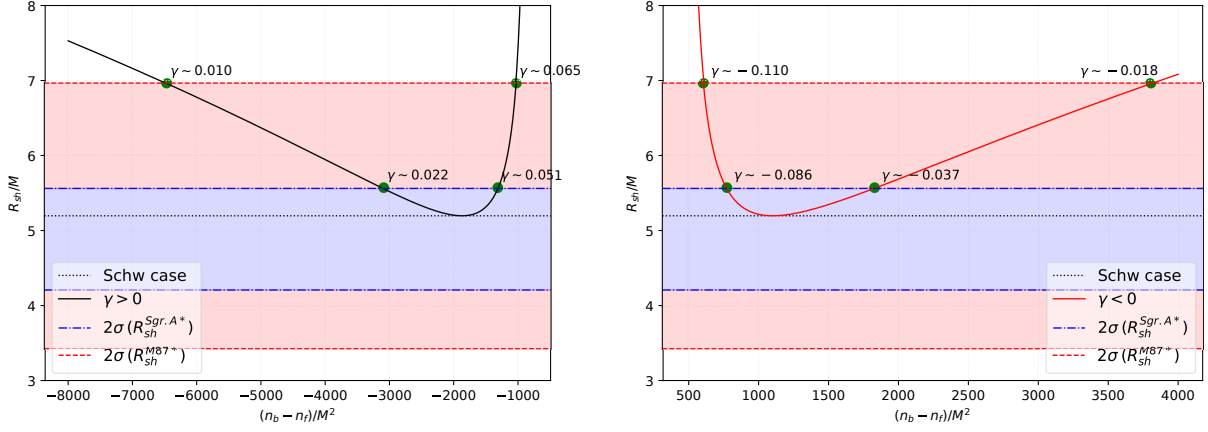


FIG. 9. The radius of the shadow of the symmergent black hole for $n_B - n_F < 0$ (left panel) and $n_B - n_F > 0$ (right panel). The dashed line is the shadow of the Schwarzschild black hole. Superimposed 1σ and 2σ bands follow from the Sgr. A* observational data in Table I. The minimal shadow radii ($R_{sh} = 3\sqrt{3}$) around $n_b - n_f \approx -2000$ (left) and $n_b - n_f \approx 1100$ (right) fall into the allowed domains (blue) in Fig. 4.

rapid fall-off with the impact parameter. It is with fairly small impact parameters ($b \gtrsim 6$) that one starts discriminating different $n_B - n_F$ values.

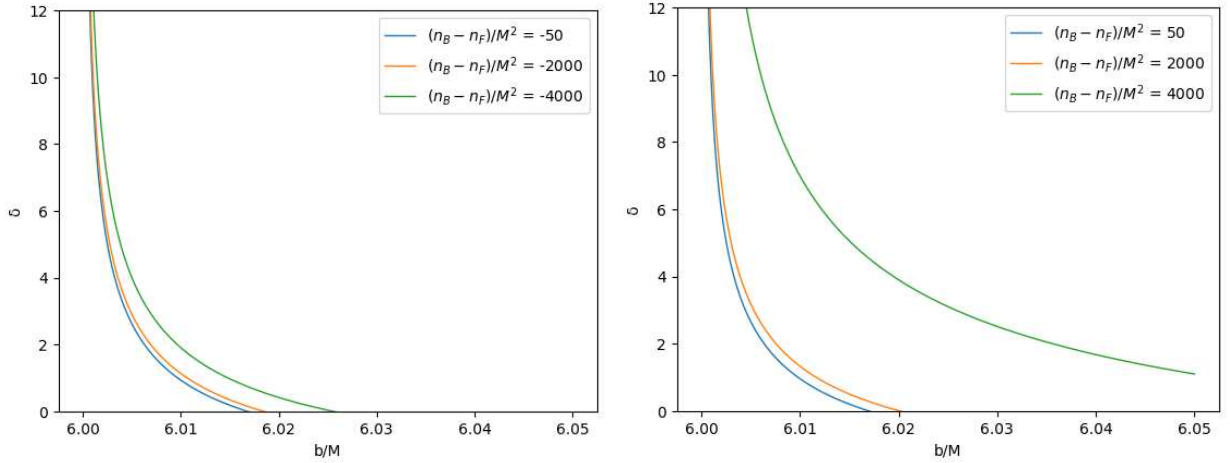


FIG. 10. Weak deflection angle from the symmergent black hole as a function of the impact parameter for $n_B - n_F < 0$ (left panel) and $n_B - n_F > 0$ (right panel).

VI. CONCLUSION

Symmergent gravity is an emergent gravity theory with $R + R^2$ curvature sector and a new particle sector. In the present work, we have constructed and analyzed asymptotically flat, static, spherically-symmetric symmergent gravity black holes. In the case of constant scalar curvature, the quadratic curvature term (coefficient of R^2) does not affect the asymptotically flat spacetimes [77–79]. In the case of variable scalar curvature, however, there arise asymptotically-flat solutions with explicit dependence on the quadratic curvature term [80] (see also [81, 82]). In the present work, we have studied such variable-scalar-curvature black holes in detail.

In Sec. II, we have a detailed discussion of the symmergent gravity [1, 2] regarding its new particles (symmeron) sector (Sec. IIA) and its curvature sector (Sec. IIB). In Sec. III, we have explicitly constructed asymptotically-flat, static, spherically-symmetric symmergent gravity black holes with variable scalar curvature. Our analysis goes beyond that in [80] as we considered both positive and negative values of the boson-fermion number difference. In both cases, we have shown

the asymptotic flatness of the metric, with approximate analytic calculations and the exact numerical solutions. In Sec. IV, we have computed the Hawking temperature using the tunneling method and concluded that black hole evaporation could be accelerated if there exist light symmerons of a significant number. In Sec. V, we have analyzed how the symmergent black hole can be probed via its shadow cast and weak deflection angle. We have shown that symmergent effects on the shadow are essentially a $2 - \sigma$ effect, and the weak deflection angle can distinguish different boson-fermion number differences at fairly large impact factors.

Our analysis in this work of the symmergent gravity is completely new in view of its asymptotic flatness and in view also of its sensitivity to the quadratic curvature term (coefficient of R^2). The analysis here can be extended to other black hole properties like quasinormal modes and grey body factors. The analysis here can also be extended by iterating Nguyen's solution to quadratic and higher-powers of the conformal factor.

ACKNOWLEDGMENTS

The work of B. P. is supported by Sabancı University, Faculty of Engineering and Natural Sciences by Faculty Post-doctoral Researcher Grant. B. P., R. P. and A. Ö. would like to acknowledge networking support by the COST Action CA18108 - Quantum gravity phenomenology in the multi-messenger approach (QG-MM). B. P., A. Ö. and D. D. would like to acknowledge networking support by the COST Action CA21106 - COSMIC WISPerS in the Dark Universe: Theory, astrophysics and experiments (CosmicWISPerS).

-
- [1] Durmus Demir, "Gauge and Poincaré properties of the UV cutoff and UV completion in quantum field theory," *Phys. Rev. D* **107**, 105014 (2023), [arXiv:2305.01671 \[hep-th\]](#).
 - [2] Durmus Demir, "Emergent Gravity as the Eraser of Anomalous Gauge Boson Masses, and QFT-GR Concord," *Gen. Rel. Grav.* **53**, 22 (2021), [arXiv:2101.12391 \[gr-qc\]](#).
 - [3] Durmus Demir, "Symmergent Gravity, Seesawic New Physics, and their Experimental Signatures," *Adv. High Energy Phys.* **2019**, 4652048 (2019), [arXiv:1901.07244 \[hep-ph\]](#).
 - [4] Durmus Ali Demir, "Curvature-Restored Gauge Invariance and Ultraviolet Naturalness," *Adv. High Energy Phys.* **2016**, 6727805 (2016), [arXiv:1605.00377 \[hep-ph\]](#).
 - [5] Philip W. Anderson, "Plasmons, Gauge Invariance, and Mass," *Phys. Rev.* **130**, 439–442 (1963).
 - [6] F. Englert and R. Brout, "Broken Symmetry and the Mass of Gauge Vector Mesons," *Phys. Rev. Lett.* **13**, 321–323 (1964).
 - [7] Peter W. Higgs, "Broken Symmetries and the Masses of Gauge Bosons," *Phys. Rev. Lett.* **13**, 508–509 (1964).
 - [8] İlim İrfan Çimdiker, "Starobinsky inflation in emergent gravity," *Phys. Dark Univ.* **30**, 100736 (2020).
 - [9] İrfan Çimdiker, Durmuş Demir, and Ali Övgün, "Black hole shadow in symmergent gravity," *Phys. Dark Univ.* **34**, 100900 (2021), [arXiv:2110.11904 \[gr-qc\]](#).
 - [10] Javlon Rayimbaev, Reggie C. Pantig, Ali Övgün, Ahmadjon Abdujabbarov, and Durmuş Demir, "Quasiperiodic oscillations, weak field lensing and shadow cast around black holes in Symmergent gravity," *Annals of Physics* (2023), [10.1016/j.aop.2023.169335](#), [arXiv:2206.06599 \[gr-qc\]](#).
 - [11] Reggie C. Pantig, Ali Övgün, and Durmuş Demir, "Testing symmergent gravity through the shadow image and weak field photon deflection by a rotating black hole using the M87* and Sgr. A* results," *Eur. Phys. J. C* **83**, 250 (2023), [arXiv:2208.02969 \[gr-qc\]](#).
 - [12] Riasat Ali and Rimsha Babar and Zunaira Akhtar and Ali Övgün, "Thermodynamics and logarithmic corrections of symmergent black holes," *Results in Physics* , 106300 (2023).
 - [13] J. L. Synge, "The Escape of Photons from Gravitationally Intense Stars," *Mon. Not. Roy. Astron. Soc.* **131**, 463–466 (1966).
 - [14] J. P. Luminet, "Image of a spherical black hole with thin accretion disk," *Astron. Astrophys.* **75**, 228–235 (1979).
 - [15] Heino Falcke, Fulvio Melia, and Eric Agol, "Viewing the shadow of the black hole at the galactic center," *Astrophys. J. Lett.* **528**, L13 (2000), [arXiv:astro-ph/9912263](#).
 - [16] Kazunori Akiyama *et al.* (Event Horizon Telescope), "First M87 Event Horizon Telescope Results. V. Physical Origin of the Asymmetric Ring," *Astrophys. J. Lett.* **875**, L5 (2019), [arXiv:1906.11242 \[astro-ph.GA\]](#).
 - [17] Kazunori Akiyama *et al.* (Event Horizon Telescope), "First Sagittarius A* Event Horizon Telescope Results. I. The Shadow of the Supermassive Black Hole in the Center of the Milky Way," *Astrophys. J. Lett.* **930**, L12 (2022).
 - [18] Sushant G. Ghosh, Rahul Kumar, and Shafqat Ul Islam, "Parameters estimation and strong gravitational lensing of nonsingular Kerr-Sen black holes," *JCAP* **03**, 056 (2021), [arXiv:2011.08023 \[gr-qc\]](#).
 - [19] Alireza Allahyari, Mohsen Khodadi, Sunny Vagnozzi, and David F. Mota, "Magnetically charged black holes from non-linear electrodynamics and the Event Horizon Telescope," *JCAP* **02**, 003 (2020), [arXiv:1912.08231 \[gr-qc\]](#).
 - [20] Cosimo Bambi, Katherine Freese, Sunny Vagnozzi, and Luca Visinelli, "Testing the rotational nature of the supermassive object M87* from the circularity and size of its first image," *Phys. Rev. D* **100**, 044057 (2019), [arXiv:1904.12983 \[gr-qc\]](#).
 - [21] Sunny Vagnozzi, Rittick Roy, Yu-Dai Tsai, Luca Visinelli, Misba Afrin, Alireza Allahyari, Parth Bambhaniya, Dipanjan Dey, Sushant G Ghosh, Pankaj S. Joshi, Kimet Jusufi, Mohsen Khodadi, Rahul Kumar Walia, Ali Övgün, and Cosimo Bambi,

- “Horizon-scale tests of gravity theories and fundamental physics from the event horizon telescope image of sagittarius a*,” *Classical and Quantum Gravity* (2023), [arXiv:2205.07787 \[gr-qc\]](#).
- [22] Prashant Kocherlakota, Luciano Rezzolla, Heino Falcke, *et al.* (EHT Collaboration), “Constraints on black-hole charges with the 2017 eht observations of m87*,” *Phys. Rev. D* **103**, 104047 (2021).
- [23] Ali Övgün, İzzet Sakalli, and Joel Saavedra, “Shadow cast and Deflection angle of Kerr-Newman-Kasuya spacetime,” *JCAP* **10**, 041 (2018), [arXiv:1807.00388 \[gr-qc\]](#).
- [24] Ali Övgün and İzzet Sakalli, “Testing generalized Einstein–Cartan–Kibble–Sciama gravity using weak deflection angle and shadow cast,” *Class. Quant. Grav.* **37**, 225003 (2020), [arXiv:2005.00982 \[gr-qc\]](#).
- [25] Ali Övgün, İzzet Sakalli, Joel Saavedra, and Carlos Leiva, “Shadow cast of noncommutative black holes in Rastall gravity,” *Mod. Phys. Lett. A* **35**, 2050163 (2020), [arXiv:1906.05954 \[hep-th\]](#).
- [26] Xiao-Mei Kuang and Ali Övgün, “Strong gravitational lensing and shadow constraint from M87* of slowly rotating Kerr-like black hole,” (2022), [arXiv:2205.11003 \[gr-qc\]](#).
- [27] Yashmitha Kumaran and Ali Övgün, “Deflection Angle and Shadow of the Reissner–Nordström Black Hole with Higher-Order Magnetic Correction in Einstein–Nonlinear–Maxwell Fields,” *Symmetry* **14**, 2054 (2022), [arXiv:2210.00468 \[gr-qc\]](#).
- [28] Ghulam Mustafa, Farruh Atamurotov, Ibrar Hussain, Sanjar Shaymatov, and Ali Övgün, “Shadows and gravitational weak lensing by the Schwarzschild black hole in the string cloud background with quintessential field*,” *Chin. Phys. C* **46**, 125107 (2022), [arXiv:2207.07608 \[gr-qc\]](#).
- [29] Mert Okyay and Ali Övgün, “Nonlinear electrodynamics effects on the black hole shadow, deflection angle, quasinormal modes and greybody factors,” *JCAP* **01**, 009 (2022), [arXiv:2108.07766 \[gr-qc\]](#).
- [30] Farruh Atamurotov, Ibrar Hussain, Ghulam Mustafa, and Ali Övgün, “Weak deflection angle and shadow cast by the charged-Kiselev black hole with cloud of strings in plasma*,” *Chin. Phys. C* **47**, 025102 (2023).
- [31] Askar B. Abdikamalov, Ahmadjon A. Abdujabbarov, Dimitry Ayzenberg, Daniele Malafarina, Cosimo Bambi, and Bobomurat Ahmedov, “Black hole mimicker hiding in the shadow: Optical properties of the γ metric,” *Phys. Rev. D* **100**, 024014 (2019), [arXiv:1904.06207 \[gr-qc\]](#).
- [32] Ahmadjon Abdujabbarov, Bakhtinur Juraev, Bobomurat Ahmedov, and Zdeněk Stuchlík, “Shadow of rotating wormhole in plasma environment,” *Astrophys. Space Sci.* **361**, 226 (2016).
- [33] Farruh Atamurotov and Bobomurat Ahmedov, “Optical properties of black hole in the presence of plasma: shadow,” *Phys. Rev. D* **92**, 084005 (2015), [arXiv:1507.08131 \[gr-qc\]](#).
- [34] Uma Papnoi, Farruh Atamurotov, Sushant G. Ghosh, and Bobomurat Ahmedov, “Shadow of five-dimensional rotating Myers-Perry black hole,” *Phys. Rev. D* **90**, 024073 (2014), [arXiv:1407.0834 \[gr-qc\]](#).
- [35] Ahmadjon Abdujabbarov, Farruh Atamurotov, Yusuf Kucukakca, Bobomurat Ahmedov, and Ugur Camci, “Shadow of Kerr-Taub-NUT black hole,” *Astrophys. Space Sci.* **344**, 429–435 (2013), [arXiv:1212.4949 \[physics.gen-ph\]](#).
- [36] Farruh Atamurotov, Ahmadjon Abdujabbarov, and Bobomurat Ahmedov, “Shadow of rotating non-Kerr black hole,” *Phys. Rev. D* **88**, 064004 (2013).
- [37] Pedro V. P. Cunha and Carlos A. R. Herdeiro, “Shadows and strong gravitational lensing: a brief review,” *Gen. Rel. Grav.* **50**, 42 (2018), [arXiv:1801.00860 \[gr-qc\]](#).
- [38] Samuel E. Gralla, Daniel E. Holz, and Robert M. Wald, “Black Hole Shadows, Photon Rings, and Lensing Rings,” *Phys. Rev. D* **100**, 024018 (2019), [arXiv:1906.00873 \[astro-ph.HE\]](#).
- [39] A. Belhaj, H. Belmahi, M. Benali, W. El Hadri, H. El Moumni, and E. Torrente-Lujan, “Shadows of 5D black holes from string theory,” *Phys. Lett. B* **812**, 136025 (2021), [arXiv:2008.13478 \[hep-th\]](#).
- [40] A. Belhaj, M. Benali, A. El Balali, H. El Moumni, and S. E. Ennadifi, “Deflection angle and shadow behaviors of quintessential black holes in arbitrary dimensions,” *Class. Quant. Grav.* **37**, 215004 (2020), [arXiv:2006.01078 \[gr-qc\]](#).
- [41] R. A. Konoplya, “Shadow of a black hole surrounded by dark matter,” *Phys. Lett. B* **795**, 1–6 (2019), [arXiv:1905.00064 \[gr-qc\]](#).
- [42] Shao-Wen Wei, Yuan-Chuan Zou, Yu-Xiao Liu, and Robert B. Mann, “Curvature radius and Kerr black hole shadow,” *JCAP* **08**, 030 (2019), [arXiv:1904.07710 \[gr-qc\]](#).
- [43] Ru Ling, Hong Guo, Hang Liu, Xiao-Mei Kuang, and Bin Wang, “Shadow and near-horizon characteristics of the acoustic charged black hole in curved spacetime,” *Phys. Rev. D* **104**, 104003 (2021), [arXiv:2107.05171 \[gr-qc\]](#).
- [44] Rahul Kumar, Sushant G. Ghosh, and Anzhong Wang, “Gravitational deflection of light and shadow cast by rotating Kalb-Ramond black holes,” *Phys. Rev. D* **101**, 104001 (2020), [arXiv:2001.00460 \[gr-qc\]](#).
- [45] Rahul Kumar and Sushant G. Ghosh, “Accretion onto a noncommutative geometry inspired black hole,” *European Physical Journal C* **77**, 577 (2017), [arXiv:1703.10479 \[gr-qc\]](#).
- [46] Pedro V. P. Cunha, Carlos A. R. Herdeiro, Burkhard Kleihaus, Jutta Kunz, and Eugen Radu, “Shadows of Einstein–dilaton–Gauss–Bonnet black holes,” *Phys. Lett. B* **768**, 373–379 (2017), [arXiv:1701.00079 \[gr-qc\]](#).
- [47] Pedro V. P. Cunha, Carlos A. R. Herdeiro, Eugen Radu, and Helgi F. Runarsson, “Shadows of Kerr black holes with and without scalar hair,” *Int. J. Mod. Phys. D* **25**, 1641021 (2016), [arXiv:1605.08293 \[gr-qc\]](#).
- [48] P. V. P. Cunha, J. Grover, C. Herdeiro, E. Radu, H. Runarsson, and A. Wittig, “Chaotic lensing around boson stars and Kerr black holes with scalar hair,” *Phys. Rev. D* **94**, 104023 (2016), [arXiv:1609.01340 \[gr-qc\]](#).
- [49] Alexander F. Zakharov, “Constraints on a charge in the Reissner–Nordström metric for the black hole at the Galactic Center,” *Phys. Rev. D* **90**, 062007 (2014), [arXiv:1407.7457 \[gr-qc\]](#).
- [50] Naoki Tsukamoto, “Black hole shadow in an asymptotically-flat, stationary, and axisymmetric spacetime: The Kerr–Newman and rotating regular black holes,” *Phys. Rev. D* **97**, 064021 (2018), [arXiv:1708.07427 \[gr-qc\]](#).
- [51] L. Chakhchi, H. El Moumni, and K. Masmar, “Shadows and optical appearance of a power-Yang–Mills black hole surrounded by different accretion disk profiles,” *Phys. Rev. D* **105**, 064031 (2022).

- [52] Peng-Cheng Li, Minyong Guo, and Bin Chen, “Shadow of a Spinning Black Hole in an Expanding Universe,” *Phys. Rev. D* **101**, 084041 (2020), [arXiv:2001.04231 \[gr-qc\]](#).
- [53] Prashant Kocherlakota *et al.* (Event Horizon Telescope), “Constraints on black-hole charges with the 2017 EHT observations of M87*,” *Phys. Rev. D* **103**, 104047 (2021), [arXiv:2105.09343 \[gr-qc\]](#).
- [54] Reggie C. Pantig and Ali Övgün, “Testing dynamical torsion effects on the charged black hole’s shadow, deflection angle and greybody with M87* and Sgr. A* from EHT,” *Annals Phys.* **448**, 169197 (2023), [arXiv:2206.02161 \[gr-qc\]](#).
- [55] Reggie C. Pantig, Leonardo Mastrototaro, Gaetano Lambiase, and Ali Övgün, “Shadow, lensing, quasinormal modes, greybody bounds and neutrino propagation by dyonic ModMax black holes,” *Eur. Phys. J. C* **82**, 1155 (2022), [arXiv:2208.06664 \[gr-qc\]](#).
- [56] Nikko John Leo S. Lobos and Reggie C. Pantig, “Generalized extended uncertainty principle black holes: Shadow and lensing in the macro- and microscopic realms,” *Physics* **4**, 1318–1330 (2022).
- [57] Akhil Uniyal, Reggie C. Pantig, and Ali Övgün, “Probing a non-linear electrodynamics black hole with thin accretion disk, shadow, and deflection angle with M87* and Sgr A* from EHT,” *Phys. Dark Univ.* **40**, 101178 (2023), [arXiv:2205.11072 \[gr-qc\]](#).
- [58] Ali Övgün, Reggie C. Pantig, and Ángel Rincón, “4D scale-dependent Schwarzschild-AdS/dS black holes: study of shadow and weak deflection angle and greybody bounding,” *Eur. Phys. J. Plus* **138**, 192 (2023), [arXiv:2303.01696 \[gr-qc\]](#).
- [59] Akhil Uniyal, Sayan Chakrabarti, Reggie C. Pantig, and Ali Övgün, “Nonlinearly charged black holes: Shadow and Thin-accretion disk,” (2023), [arXiv:2303.07174 \[gr-qc\]](#).
- [60] Grigoris Panotopoulos, Ángel Rincón, and Ildio Lopes, “Orbits of light rays in scale-dependent gravity: Exact analytical solutions to the null geodesic equations,” *Phys. Rev. D* **103**, 104040 (2021), [arXiv:2104.13611 \[gr-qc\]](#).
- [61] Grigoris Panotopoulos and Angel Rincon, “Orbits of light rays in (12)-dimensional Einstein–power–Maxwell gravity: Exact analytical solution to the null geodesic equations,” *Annals Phys.* **443**, 168947 (2022), [arXiv:2206.03437 \[gr-qc\]](#).
- [62] Mohsen Khodadi and Gaetano Lambiase, “Probing Lorentz symmetry violation using the first image of Sagittarius A*: Constraints on standard-model extension coefficients,” *Phys. Rev. D* **106**, 104050 (2022), [arXiv:2206.08601 \[gr-qc\]](#).
- [63] Mohsen Khodadi, Gaetano Lambiase, and David F. Mota, “No-hair theorem in the wake of Event Horizon Telescope,” *JCAP* **09**, 028 (2021), [arXiv:2107.00834 \[gr-qc\]](#).
- [64] Yuan Meng, Xiao-Mei Kuang, Xi-Jing Wang, and Jian-Pin Wu, “Shadow revisiting and weak gravitational lensing with Chern-Simons modification,” (2023), [10.1016/j.physletb.2023.137940](#), [arXiv:2305.04210 \[gr-qc\]](#).
- [65] Rajibul Shaikh, “Testing black hole mimickers with the Event Horizon Telescope image of Sagittarius A*,” (2022), [10.1093/mnras/stad1383](#), [arXiv:2208.01995 \[gr-qc\]](#).
- [66] Rajibul Shaikh, Suvankar Paul, Pritam Banerjee, and Tapobrata Sarkar, “Shadows and thin accretion disk images of the γ -metric,” *Eur. Phys. J. C* **82**, 696 (2022), [arXiv:2105.12057 \[gr-qc\]](#).
- [67] Rajibul Shaikh, Prashant Kocherlakota, Ramesh Narayan, and Pankaj S. Joshi, “Shadows of spherically symmetric black holes and naked singularities,” *Mon. Not. Roy. Astron. Soc.* **482**, 52–64 (2019), [arXiv:1802.08060 \[astro-ph.HE\]](#).
- [68] Rajibul Shaikh and Pankaj S. Joshi, “Can we distinguish black holes from naked singularities by the images of their accretion disks?” *JCAP* **10**, 064 (2019), [arXiv:1909.10322 \[gr-qc\]](#).
- [69] Reggie C. Pantig and Ali Övgün, “Dehnen halo effect on a black hole in an ultra-faint dwarf galaxy,” *JCAP* **08**, 056 (2022), [arXiv:2202.07404 \[astro-ph.GA\]](#).
- [70] Reggie C. Pantig and Ali Övgün, “Black hole in quantum wave dark matter,” *Fortsch. Phys.* **2022**, 2200164 (2022), [arXiv:2210.00523 \[gr-qc\]](#).
- [71] Reggie C. Pantig, “Constraining a one-dimensional wave-type gravitational wave parameter through the shadow of M87* via Event Horizon Telescope,” (2023), [arXiv:2303.01698 \[gr-qc\]](#).
- [72] Mingzhi Wang, Songbai Chen, and Jiliang Jing, “Effect of gravitational wave on shadow of a Schwarzschild black hole,” *Eur. Phys. J. C* **81**, 509 (2021), [arXiv:1908.04527 \[gr-qc\]](#).
- [73] Rittick Roy and Sayan Chakrabarti, “Study on black hole shadows in asymptotically de Sitter spacetimes,” *Phys. Rev. D* **102**, 024059 (2020), [arXiv:2003.14107 \[gr-qc\]](#).
- [74] R. A. Konoplya, “Black holes in galactic centers: Quasinormal ringing, grey-body factors and Unruh temperature,” *Phys. Lett. B* **823**, 136734 (2021), [arXiv:2109.01640 \[gr-qc\]](#).
- [75] Arshia Anjum, Misba Afrin, and Sushant G. Ghosh, “Astrophysical consequences of dark matter for photon orbits and shadows of supermassive black holes,” (2023), [arXiv:2301.06373 \[gr-qc\]](#).
- [76] Xian Hou, Zhaoyi Xu, Ming Zhou, and Jiancheng Wang, “Black hole shadow of Sgr A* in dark matter halo,” *JCAP* **07**, 015 (2018), [arXiv:1804.08110 \[gr-qc\]](#).
- [77] William Nelson, “Static Solutions for 4th order gravity,” *Phys. Rev. D* **82**, 104026 (2010), [arXiv:1010.3986 \[gr-qc\]](#).
- [78] H. Lu, A. Perkins, C. N. Pope, and K. S. Stelle, “Black Holes in Higher-Derivative Gravity,” *Phys. Rev. Lett.* **114**, 171601 (2015), [arXiv:1502.01028 \[hep-th\]](#).
- [79] H. Lü, A. Perkins, C. N. Pope, and K. S. Stelle, “Spherically Symmetric Solutions in Higher-Derivative Gravity,” *Phys. Rev. D* **92**, 124019 (2015), [arXiv:1508.00010 \[hep-th\]](#).
- [80] Hoang Ky Nguyen, “Beyond Schwarzschild-de Sitter spacetimes: III. A perturbative vacuo with non-constant scalar curvature in $R + R^2$ gravity,” (2022), [arXiv:2211.07380 \[gr-qc\]](#).
- [81] Hoang Ky Nguyen, “Beyond Schwarzschild–de Sitter spacetimes: A new exhaustive class of metrics inspired by Buchdahl for pure R^2 gravity in a compact form,” *Phys. Rev. D* **106**, 104004 (2022), [arXiv:2211.01769 \[gr-qc\]](#).
- [82] Hoang Ky Nguyen, “Beyond Schwarzschild-de Sitter spacetimes: II. An exact non-Schwarzschild metric in pure R^2 gravity and new anomalous properties of R^2 black holes,” (2022), [arXiv:2211.03542 \[gr-qc\]](#).

- [83] Alfredo Macias and Abel Camacho, "On the incompatibility between quantum theory and general relativity," *Phys. Lett. B* **663**, 99–102 (2008).
- [84] Robert M. Wald, "The Formulation of Quantum Field Theory in Curved Spacetime," *Einstein Stud.* **14**, 439–449 (2018), [arXiv:0907.0416 \[gr-qc\]](#).
- [85] Freeman Dyson, "Is a graviton detectable?" *Int. J. Mod. Phys. A* **28**, 1330041 (2013).
- [86] Gerard 't Hooft and M. J. G. Veltman, "One loop divergencies in the theory of gravitation," *Ann. Inst. H. Poincaré Phys. Théor.* **A 20**, 69–94 (1974).
- [87] A. D. Sakharov, "Vacuum quantum fluctuations in curved space and the theory of gravitation," *Dokl. Akad. Nauk Ser. Fiz.* **177**, 70–71 (1967).
- [88] Matt Visser, "Sakharov's induced gravity: A Modern perspective," *Mod. Phys. Lett. A* **17**, 977–992 (2002), [arXiv:gr-qc/0204062](#).
- [89] Erik P. Verlinde, "Emergent Gravity and the Dark Universe," *SciPost Phys.* **2**, 016 (2017), [arXiv:1611.02269 \[hep-th\]](#).
- [90] C. D. Froggatt and H. B. Nielsen, "Derivation of Poincaré invariance from general quantum field theory," *Annalen Phys.* **517**, 115 (2005), [arXiv:hep-th/0501149](#).
- [91] Joseph Polchinski, "Renormalization and Effective Lagrangians," *Nucl. Phys. B* **231**, 269–295 (1984).
- [92] H. Umezawa, J. Yukawa, and E. Yamada, "The problem of vacuum polarization," *Prog. Theor. Phys.* **3**, 317–318 (1948).
- [93] Gunnar Kallen, "Higher Approximations in the external field for the Problem of Vacuum Polarization," *Helv. Phys. Acta* **22**, 637–654 (1949).
- [94] Vincenzo Vitagliano, Thomas P. Sotiriou, and Stefano Liberati, "The dynamics of metric-affine gravity," *Annals Phys.* **326**, 1259–1273 (2011), [Erratum: *Annals Phys.* **329**, 186–187 (2013)], [arXiv:1008.0171 \[gr-qc\]](#).
- [95] Canan N. Karahan, Asli Altas, and Durmus A. Demir, "Scalars, Vectors and Tensors from Metric-Affine Gravity," *Gen. Rel. Grav.* **45**, 319–343 (2013), [arXiv:1110.5168 \[gr-qc\]](#).
- [96] Durmuş Demir and Beyhan Pulice, "Geometric Dark Matter," *JCAP* **04**, 051 (2020), [arXiv:2001.06577 \[hep-ph\]](#).
- [97] Durmus Demir, "Naturally-Coupled Dark Sectors," *Galaxies* **9**, 33 (2021), [arXiv:2105.04277 \[hep-ph\]](#).
- [98] Stefania Gori *et al.*, "Dark Sector Physics at High-Intensity Experiments," (2022), [arXiv:2209.04671 \[hep-ph\]](#).
- [99] J. Beacham *et al.*, "Physics Beyond Colliders at CERN: Beyond the Standard Model Working Group Report," *J. Phys. G* **47**, 010501 (2020), [arXiv:1901.09966 \[hep-ex\]](#).
- [100] Elcio Abdalla and Alessandro Marins, "The Dark Sector Cosmology," *Int. J. Mod. Phys. D* **29**, 2030014 (2020), [arXiv:2010.08528 \[gr-qc\]](#).
- [101] Juliette Alimena *et al.*, "Searching for long-lived particles beyond the Standard Model at the Large Hadron Collider," *J. Phys. G* **47**, 090501 (2020), [arXiv:1903.04497 \[hep-ex\]](#).
- [102] Gerard 't Hooft, "Dimensional reduction in quantum gravity," *Conf. Proc. C* **930308**, 284–296 (1993), [arXiv:gr-qc/9310026](#).
- [103] Andrew G. Cohen, David B. Kaplan, and Ann E. Nelson, "Effective field theory, black holes, and the cosmological constant," *Phys. Rev. Lett.* **82**, 4971–4974 (1999), [arXiv:hep-th/9803132](#).
- [104] N. D. Birrell and P. C. W. Davies, *Quantum Fields in Curved Space*, Cambridge Monographs on Mathematical Physics (Cambridge Univ. Press, Cambridge, UK, 1984).
- [105] K. Srinivasan and T. Padmanabhan, "Particle production and complex path analysis," *Phys. Rev. D* **60**, 024007 (1999), [arXiv:gr-qc/9812028](#).
- [106] Marco Angheben, Mario Nadalini, Luciano Vanzo, and Sergio Zerbini, "Hawking radiation as tunneling for extremal and rotating black holes," *JHEP* **05**, 014 (2005), [arXiv:hep-th/0503081](#).
- [107] P. Mitra, "Hawking temperature from tunnelling formalism," *Phys. Lett. B* **648**, 240–242 (2007), [arXiv:hep-th/0611265](#).
- [108] Emil T. Akhmedov, Valeria Akhmedova, and Douglas Singleton, "Hawking temperature in the tunneling picture," *Phys. Lett. B* **642**, 124–128 (2006), [arXiv:hep-th/0608098](#).
- [109] R. V. Maluf and Juliano C. S. Neves, "Thermodynamics of a class of regular black holes with a generalized uncertainty principle," *Phys. Rev. D* **97**, 104015 (2018), [arXiv:1801.02661 \[gr-qc\]](#).
- [110] P. A. González, Ali Övgün, Joel Saavedra, and Yerko Vásquez, "Hawking radiation and propagation of massive charged scalar field on a three-dimensional Gödel black hole," *Gen. Rel. Grav.* **50**, 62 (2018), [arXiv:1711.01865 \[gr-qc\]](#).
- [111] A. Övgün, "Entangled Particles Tunneling From a Schwarzschild Black Hole immersed in an Electromagnetic Universe with GUP," *Int. J. Theor. Phys.* **55**, 2919–2927 (2016), [arXiv:1508.04100 \[gr-qc\]](#).
- [112] A. Övgün and Kimet Jusufi, "The effect of the GUP on massive vector and scalar particles tunneling from a warped DGP gravity black hole," *Eur. Phys. J. Plus* **132**, 298 (2017), [arXiv:1703.08073 \[physics.gen-ph\]](#).
- [113] Ganim Gecim and Yusuf Sucu, "Tunnelling of relativistic particles from new type black hole in new massive gravity," *JCAP* **02**, 023 (2013).
- [114] M. Hossain Ali, "Hawking radiation via tunneling from hot NUT-Kerr-Newman-Kasuya spacetime," *Class. Quant. Grav.* **24**, 5849–5860 (2007), [arXiv:0706.3890 \[gr-qc\]](#).
- [115] Ryan Kerner and Robert B. Mann, "Fermions tunnelling from black holes," *Class. Quant. Grav.* **25**, 095014 (2008), [arXiv:0710.0612 \[hep-th\]](#).
- [116] Wajiha Javed, Rimsha Babar, and Ali Övgün, "Hawking radiation from cubic and quartic black holes via tunneling of GUP corrected scalar and fermion particles," *Mod. Phys. Lett. A* **34**, 1950057 (2019), [arXiv:1808.09795 \[physics.gen-ph\]](#).
- [117] Muhammad Rizwan, Muhammad Zubair Ali, and Ali Övgün, "Charged fermions tunneling from stationary axially symmetric black holes with generalized uncertainty principle," *Mod. Phys. Lett. A* **34**, 1950184 (2019), [arXiv:1812.01983 \[physics.gen-ph\]](#).
- [118] Deyou Chen, "Dirac particles' tunneling from five-dimensional rotating black strings influenced by the generalized uncertainty principle," *Eur. Phys. J. C* **74**, 2687 (2014), [arXiv:1312.2075 \[hep-th\]](#).

- [119] Ganim Gecim and Yusuf Sucu, "Quantum gravity effect on the Hawking radiation of spinning dilaton black hole," *Eur. Phys. J. C* **79**, 882 (2019).
- [120] Ran Li and Ji-Rong Ren, "Dirac particles tunneling from BTZ black hole," *Phys. Lett. B* **661**, 370–372 (2008), [arXiv:0802.3954 \[gr-qc\]](#).
- [121] M. Sharif and Wajiha Javed, "Fermions Tunneling from Charged Accelerating and Rotating Black Holes with NUT Parameter," *Eur. Phys. J. C* **72**, 1997 (2012), [arXiv:1206.2591 \[gr-qc\]](#).
- [122] Deyou Chen, Houwen Wu, and Haitang Yang, "Observing remnants by fermions' tunneling," *JCAP* **03**, 036 (2014), [arXiv:1307.0172 \[gr-qc\]](#).
- [123] S. I. Kruglov, "Black hole emission of vector particles in (1+1) dimensions," *Int. J. Mod. Phys. A* **29**, 1450118 (2014), [arXiv:1408.6561 \[gr-qc\]](#).
- [124] I. Sakalli and A. Ovgun, "Tunnelling of vector particles from Lorentzian wormholes in 3+1 dimensions," *Eur. Phys. J. Plus* **130**, 110 (2015), [arXiv:1505.02093 \[gr-qc\]](#).
- [125] Wajiha Javed, Riasat Ali, Rimsha Babar, and Ali Övgün, "Tunneling of Massive Vector Particles from Types of BTZ-like Black Holes," *Eur. Phys. J. Plus* **134**, 511 (2019), [arXiv:1910.07949 \[gr-qc\]](#).
- [126] A. Övgün and I. Sakalli, "Eruptive Massive Vector Particles of 5-Dimensional Kerr-Gödel Spacetime," *Int. J. Theor. Phys.* **57**, 322–328 (2018), [arXiv:1705.00061 \[gr-qc\]](#).
- [127] I. Sakalli and A. Övgün, "Quantum Tunneling of Massive Spin-1 Particles From Non-stationary Metrics," *Gen. Rel. Grav.* **48**, 1 (2016), [arXiv:1507.01753 \[gr-qc\]](#).
- [128] Xiao-Mei Kuang, Joel Saavedra, and Ali Övgün, "The Effect of the Gauss-Bonnet term to Hawking Radiation from arbitrary dimensional Black Brane," *Eur. Phys. J. C* **77**, 613 (2017), [arXiv:1707.00169 \[gr-qc\]](#).
- [129] T. Ibingochouba Singh, I. Ablu Meitei, and K. Yugindro Singh, "Hawking radiation as tunneling of vector particles from Kerr-Newman black hole," *Astrophys. Space Sci.* **361**, 103 (2016).
- [130] Julien Grain and A. Barrau, "A WKB approach to scalar fields dynamics in curved space-time," *Nucl. Phys. B* **742**, 253–274 (2006), [arXiv:hep-th/0603042](#).
- [131] Ryan Kerner and Robert B. Mann, "Tunnelling, temperature and Taub-NUT black holes," *Phys. Rev. D* **73**, 104010 (2006), [arXiv:gr-qc/0603019](#).
- [132] A. Övgün, "The Bekenstein-Hawking Corpuscular Cascading from the Back-Reacted Black Hole," *Adv. High Energy Phys.* **2017**, 1573904 (2017), [arXiv:1609.07804 \[gr-qc\]](#).
- [133] Don N. Page, "Particle Emission Rates from a Black Hole: Massless Particles from an Uncharged, Nonrotating Hole," *Phys. Rev. D* **13**, 198–206 (1976).
- [134] Michael J. Baker and Andrea Thamm, "Black hole evaporation beyond the Standard Model of particle physics," *JHEP* **01**, 063 (2023), [arXiv:2210.02805 \[hep-ph\]](#).
- [135] Andrew Cheek, Lucien Heurtier, Yuber F. Perez-Gonzalez, and Jessica Turner, "Primordial black hole evaporation and dark matter production. I. Solely Hawking radiation," *Phys. Rev. D* **105**, 015022 (2022), [arXiv:2107.00013 \[hep-ph\]](#).
- [136] S. W. Hawking, "Particle Creation by Black Holes," *Commun. Math. Phys.* **43**, 199–220 (1975), [Erratum: *Commun. Math. Phys.* 46, 206 (1976)].
- [137] Yves Decanini, Gilles Esposito-Farese, and Antoine Folacci, "Universality of high-energy absorption cross sections for black holes," *Phys. Rev. D* **83**, 044032 (2011), [arXiv:1101.0781 \[gr-qc\]](#).
- [138] Hao Liao, Songbai Chen, and Jiliang Jing, "Absorption cross section and Hawking radiation of the electromagnetic field with Weyl corrections," *Phys. Lett. B* **728**, 457–461 (2014), [arXiv:1312.1144 \[gr-qc\]](#).
- [139] Bahram Mashhoon, "Scattering of Electromagnetic Radiation from a Black Hole," *Phys. Rev. D* **7**, 2807–2814 (1973).
- [140] Shao-Wen Wei and Yu-Xiao Liu, "Observing the shadow of Einstein-Maxwell-Dilaton-Axion black hole," *JCAP* **11**, 063 (2013), [arXiv:1311.4251 \[gr-qc\]](#).
- [141] Volker Perlick and Oleg Yu. Tsupko, "Calculating black hole shadows: Review of analytical studies," *Phys. Rept.* **947**, 1–39 (2022), [arXiv:2105.07101 \[gr-qc\]](#).
- [142] Dimitrios Psaltis *et al.* (Event Horizon Telescope), "Gravitational Test Beyond the First Post-Newtonian Order with the Shadow of the M87 Black Hole," *Phys. Rev. Lett.* **125**, 141104 (2020), [arXiv:2010.01055 \[gr-qc\]](#).
- [143] Steven Weinberg, *Gravitation and Cosmology: Principles and Applications of the General Theory of Relativity* (John Wiley and Sons, New York, 1972).
- [144] Xu Lu and Yi Xie, "Weak and strong deflection gravitational lensing by a renormalization group improved Schwarzschild black hole," *Eur. Phys. J. C* **79**, 1016 (2019).
- [145] K. S. Virbhadra, D. Narasimha, and S. M. Chitre, "Role of the scalar field in gravitational lensing," *Astron. Astrophys.* **337**, 1–8 (1998), [arXiv:astro-ph/9801174](#).